Estimating Soil Parameters From Hyperspectral Images: A benchmark dataset and the outcome of the HYPERVIEW challenge

Estimating Soil Parameters from Hyperspectral Images: A Benchmark Dataset and the Outcome of the HYPERVIEW Challenge

Journal:	*IEEE Geoscience and Remote Sensing Magazine*
Manuscript ID	GRSM-2023-00081.R2
Manuscript Type:	Review Paper
Date Submitted by the Author:	n/a
Complete List of Authors:	Nalepa, Jakub; Politechnika Slaska, Institute of Informatics Tulczyjew, Lukasz; KP Labs, Earth Observation Group Le Saux, Bertrand; ESRIN, Phi lab Longépé, Nicolas; ESRIN, Φ-lab Explore Office Ruszczak, Bogdan; KP Labs, Earth Observation Group Wijata, Agata; Silesian University of Technology, Faculty of Biomedical Engineering Smykala, Krzysztof; QZ Solutions Sp z oo, Research and Development Department Myller, Michal; KP Labs, Earth Observation Group Kawulok, Michal; Politechnika Slaska, Institute of Informatics Kuzu, Ridvan Salih ; DLR Oberpfaffenhofen, Earth Observation Center Albrecht, Frauke; German Climate Computing Centre, DKRZ Arnold, Caroline; German Climate Computing Centre, Applications Alasawedah, Mohammad; EURAC Research, Institute for Earth Observation Angeli, Suzanne; Capgemini Application Services, Cloud & Custom Applications Nobileau, Delphine; Capgemini Application Services, Cloud & Custom Applications Ballabeni, Achille; Alma Mater Studiorum Università di Bologna, Department of Industrial Engineering Lotti, Alessandro; Alma Mater Studiorum Università di Bologna, Department of Industrial Engineering Locarini, Alfredo; Alma Mater Studiorum Università di Bologna, Department of Industrial Engineering Modenini, Dario; Alma Mater Studiorum Università di Bologna, Department of Industrial Engineering Tortora, Paolo; Università di Bologna, DIEM Gumiela, Michal; KP Labs, Systems Engineering Department
Keywords:	Hyperspectral imaging, Machine learning algorithms, Soil properties, Artificial intelligence

Estimating Soil Parameters from Hyperspectral Images: A Benchmark Dataset and the Outcome of the HYPERVIEW Challenge

Jakub Nalepa, *Senior Member, IEEE*, Lukasz Tulczyjew, Bertrand Le Saux, *Senior Member, IEEE*, Nicolas Longépé, Bogdan Ruszczak, Agata M. Wijata, *Member, IEEE*, Krzysztof Smykala, Michal Myller, Michal Kawulok, *Senior Member, IEEE*, Rıdvan Salih Kuzu, Frauke Albrecht, Caroline Arnold, Mohammad Alasawedah, Suzanne Angeli, Delphine Nobileau, Achille Ballabeni, Alessandro Lotti, Alfredo Locarini, Dario Modenini, *Member, IEEE*, Paolo Tortora, *Senior Member, IEEE*, and Michal Gumiela

***Abstract*—Enhancing agricultural methods through the utilization of Earth observation and artificial intelligence (AI) has emerged as a significant concern. The ability to quantify soil parameters on a large scale can play a pivotal role in optimizing the fertilization process. While techniques for non-invasive estimation of soil parameters from hyperspectral images exist, their validation typically occurs across different datasets and employs varying validation protocols. This diversity renders them inherently challenging (or even impossible) to compare objectively. We address this research gap and introduce an AI-ready dataset containing airborne hyperspectral images collocated with in-situ measurements of phosphorus pentoxide, potassium oxide, magnesium, and soil pH. Furthermore, we propose a standardized validation procedure to adhere to when assessing the performance of the emerging algorithms for estimating soil parameters. This dataset was utilized in the HYPERVIEW: "*Seeing Beyond the Visible*" challenge, with the goal of deploying data-driven soil analysis algorithms on board Intuition-1—a satellite equipped with a hyperspectral camera and on-board AI capabilities. In this article, we present the top-4 solutions (HYPERVIEW attracted almost 160 teams with 46 actively submitting predictions to the validation server) and provide the organizers' perspective on the challenge, its progress, statistics, and insights. To ensure reproducibility, we made the dataset available through the permanently open version of HYPERVIEW at https://platform.ai4eo.eu/seeing-beyond-the-visible-permanent. We believe that our efforts will play a crucial role in establishing a standardized approach for the validation of AI solutions, not only in the domain of soil analysis but in related fields as well.**

***Index Terms*—Benchmark, soil analysis, deep learning, machine learning, hyperspectral imaging.**

JN, LT, BR, AMW, MM, MK, MG are with KP Labs, Gliwice, Poland.
JN, LT, AMW, MK are with the Silesian University of Technology, Poland.
BLS, NL are with Φ-Lab, European Space Agency, Frascati, Italy.
KS is with QZ Solutions, Opole, Poland.
BR is with Opole University of Technology, Opole, Poland.
RSK is with German Aerospace Center (DLR), Weßling, Germany.
FA, CA are with Helmholtz AI, Oberschleißheim, Germany, German Climate Computing Centre (DKRZ), Hamburg, Germany, Helmholtz-Zentrum Hereon, Geesthacht, Germany.
MA is with Eurac Research, Institute for Earth Observation, Bolzano, Italy.
SA, DN are with Capgemini Application Services, Cloud & Custom Applications, Toulouse, France.
AB, AL, ALo, DM, PT are with Department of Industrial Engineering, Alma Mater Studiorum Università di Bologna, Forlì, Italy.
DM, PT are with Interdepartmental Centre for Industrial Research, Alma Mater Studiorum Università di Bologna, Forlì, Italy.
Corresponding author: J. Nalepa
Manuscript received April 19, 2005; revised August 26, 2015.

I. Introduction

THE agricultural sector has witnessed significant transformations, largely influenced by technological advancements [1]. With limited arable land [2], the need to enhance crop productivity to meet the nutritional demands of a growing population is critical [3]. Consequently, precision agriculture emerged as a fundamental approach for efficient food production, targeting the problem of reducing the environmental impact of agricultural practices [4]. This suite of targeted strategies includes, among others, the evaluation and monitoring of soil quality, moisture levels, fertilizer content, temperature, and seasonal ecosystem changes over time [5], [6]. Estimating planned yields for specific regions [7] also provides vital information regarding the effectiveness of implemented practices [8]. Precise monitoring of soil composition, especially soil pH, is instrumental in averting soil degradation [9].

Monitoring soil parameters traditionally involves in-situ measurements where soil samples are analyzed in laboratory conditions [10]–[12]. However, this method is associated with high costs, time inefficiency, and limited scalability over large areas [13]. Current approaches often necessitate mixing soil samples from an entire field, preventing the extraction of soil parameters for specific field segments [14]. Also, the quality of the obtained soil samples and the laboratory settings may influence the extracted parameters [15], [16]. To overcome these limitations, non-invasive imaging methods have gained traction for assessing the spatial distribution of soil components, offering improved scalability [17], [18]. To create data-driven supervised machine learning models for this task, various imagery sources, such as drones [8], [19]–[21], airborne platforms [22]–[24], or satellites [25]–[27] are combined with in-situ measurements, ideally with precise geospatial information [12], [28], to create ground-truth datasets [26], [29]. These datasets not only serve to develop models but also to assess their generalization.

However, the process of building high-quality, representative, and diverse ground-truth data is costly, not scalable, and relies on human efforts. It also requires meticulous coordination between soil sample collection and image acquisition campaigns [12], [18], [30]. Although some studies have collected in-field measurements and images within the

same month but in different years [31], [32], this can lead to inaccurate ground-truth information, especially for fertilized regions. Moreover, external factors like atmospheric conditions, weather, and seasonality [33] influence measurements, necessitating careful planning of data acquisition scenarios. Of note, various prior studies have recommended the adoption of the Mehlich 3 extractant for conducting comprehensive soil elemental analysis, with the goal of enhancing soil analysis across the globe, e.g., in the United States [34], Zimbabwe [35], China [36], Kenya [37], or Poland [38]. While this approach requires a significant amount of time, involves intricate testing procedures, and comes with elevated testing costs, it remains the state of the art in extracting soil parameters (with proven repeatability and reproducibility [15], [16])—the current efforts are focused on accelerating it and making it more affordable [39]. Given these challenges, publicly available datasets for validating data-driven algorithms to estimate soil parameters from image data are lacking.

Satellite remote sensing is a valuable tool for identifying soil composition [40], [41] and tracking changes in soil characteristics [5]. This technology offers scalability to monitor large areas [42] and to build a documented history of the area [43]. By leveraging remotely-sensed data, practitioners can optimize their practices [31]. The acquired satellite image data comes in various modalities, with multispectral images (MSIs [21], [28]) and hyperspectral images (HSIs [3], [24], [44]) commonly used in precision agriculture. Multispectral instruments capture several broad spectral bands [45], while HSI records hundreds of narrow and contiguous bands across the electromagnetic spectrum. Vegetation indices (VIs), being spectral indices derived from MSI [46], are often employed in agriculture for tasks like bare soil detection, chlorophyll monitoring, and vegetation tracking [46]–[49]. The lower spectral resolution of MSIs can limit their ability to detect subtle changes [50], such as plant diseases [51], [52]. In contrast, hyperspectral instruments with high spectral resolution [3], [13] offer new possibilities for developing algorithms to detect nutrient deficiencies, soil hydration, and other ecosystem processes [53].

Numerous agricultural parameters have been investigated in the context of extracting them from HSIs. They span across the crop volume [8], soil and crop irrigation levels [54], [55], soil temperature [6], type [56] and texture [32], its composition accompanied by the identification of minerals [57], nutrients [21], [32], organic carbon [25], [47], salinity [44], soil pH [29] or soil pollution [58]. A prompt and reliable evaluation of soil parameters is vital in resource management [4], [44], especially when applying fertilizers [3], [17]. Particular attention should be paid to the parameters that a farmer can influence by providing the soil with nutrients, such as nitrogen (N) [3], [17], [32], [40], phosphorus (P) [3], [17], [21], [32], [40], potassium (K) [3], [17], [21], [40], magnesium (Mg) [21], [32] and organic carbon (OC) [17], [32], as well as soil pH [21] affecting vegetation. The assessment of soil composition should prioritize bare soil areas due to the substantial impact on results from even small remnants of green vegetation that may remain after the harvest [22], [47].

There are prior insights concerning the spectral signatures of specific soil parameters that may be used while extracting them. The absorbance maxima for both the basic and neutral forms of bromothymol blue, a phenol-based dye often used to test pH, occur at 618 nm and 420 nm [59]. The wavelength range from 630 to 780 nm [60] is also important here. The strong lines of K are found at various wavelengths such as 441.81 nm, 465.08 nm, 476.03 nm, 495.14 nm, 600.77 nm, 607.93 nm, and 612.62 nm [61]. The atomic emission spectra of Mg are 285.21 nm, 279.55 nm, 279.81 nm, and 280.27 nm [62], and magnesium may not have a well-defined spectral signature in the 400–900 nm range. The soil pH, on the other hand, affects the spectral characteristics of various substances, which can be used to determine pH [63].

The algorithms used to extract soil parameters from image data (MSIs and HSIs) can be split into classic statistical analysis (SA) [12], [21] techniques, as well as classic and deep machine learning (ML) approaches [18], [64]. In the former group, we benefit from a range of VIs, such as the Normalized Difference Vegetation Index (NDVI), Enhanced Vegetation Index (EVI), Optimized Soil Adjusted Vegetation Index (OSAVI) [25], [32], [65], and many others [25], [32], [65] to estimate C [25], [66], P and its compounds [32], [65], K and its compounds [65], [67], and pH [33], [68]. They are calculated based on the pre-processed imagery [29] which undergoes various corrections, e.g., atmospheric [32]. In ML algorithms, we either use hand-crafted features [9], [67], [69], which are later fed to supervised learners that perform prediction [68], or benefit from automated representation learning offered by deep learning. The classic ML models used for estimating soil parameters encompass Support Vector Machines (SVMs) [24], [70], Random Forests (RFs) [3], [24], Multiple Linear Regression (MLR) models [18], Partial Least Squares Regression (PLSR) techniques [33], and a plethora of boosting strategies [32]. Deep learning algorithms have been deployed for soil parameters' estimation as well [71], and they are very often coupled with data augmentation [72] and transfer learning [73] to deal with limited ground truth.

The majority of the approaches were validated over the data captured for a selected region, commonly exploiting a single image [3], [31]. There are studies in which several dozens of images were collected [47], but this data was captured over the years, and the actual composition of the soil is not documented. Various strategies, including multi-fold cross-validation [26], [69], were used to eliminate the risk of leaking the information across the training and test sets [29], [74]. Ideally, the algorithms should be trained and validated over spatially and temporally de-correlated datasets. Incorrectly designed validation procedures lead to elaborating overly optimistic estimations of the generalization capabilities of ML models—this issue has been thoroughly investigated in our previous works [75], [76]. Finally, there are quality metrics that are used to assess the quality of automated soil estimation, with the coefficient of determination (R^2) and the root mean square error (RSME) being well-established in the field [3], [17], [70]. In the supplementary materials, we gather a tabular summary of a representative set of techniques for estimating soil parameters from different data modalities showing a notable diversity of the validation approaches. The lack of standardization of this process can, unfortunately, lead

to the "illusion of progress" in the field, as the results obtained for the emerging approaches cannot be directly compared with others, and they may not be reproducible, ultimately leading to the reproducibility crisis [77]. In this article, we address this research gap by introducing an AI-ready dataset that can be used for fair validation of such approaches.

A. Contribution

We tackle the problem of estimating soil parameters from HSIs and address the research gaps related to the data availability, unbiased and objective validation of emerging algorithms for this task, and ensuring full reproducibility of such methods. Overall, our contributions are as follows:

- We gathered real-life data, including airborne HSIs collocated with in-situ soil samples which underwent laboratory analysis to precisely extract four, practically important soil parameters: phosphorus pentoxide (P_2O_5), potassium oxide (K_2O), magnesium (Mg), and the soil pH. Knowing these parameters may help optimize agricultural management, ultimately improving the quality and quantity of crop yield.
- We designed and implemented a validation procedure, together with the AI-ready dataset, including the training-test split alongside the quantitative metrics for comparing the algorithms, and for ensuring the experimental reproducibility.
- We organized the HYPERVIEW: *"Seeing Beyond the Visible"* challenge focused on developing algorithms for estimating soil parameters from HSIs, with the goal of deploying them on board the satellite. Thanks to HYPERVIEW, we gathered the first-of-its-kind ranking of soil analysis algorithms validated over the same data and following the same validation strategy. Thus, we ensure the transparency and objectiveness of the entire process.
- We made the HYPERVIEW dataset available at https://platform.ai4eo.eu/seeing-beyond-the-visible- permanent to allow the community compare their techniques with the current state of the art, hence to monitor the progress in the field objectively.
- We discuss the top-ranked HYPERVIEW solutions (out of all 46 submitted solutions; the challenge attracted the attention of 159 registered teams from all over the world), and focus on the process of designing and verifying them. It provides the participants' perspective on the challenge.
- We provide the organizers' perspective on HYPERVIEW, its progress, various statistics, and insights, also concerning the HYPERVIEW dataset, which was not revealed to the participants during the challenge, as they might have influenced the algorithms, e.g., by injecting some additional "expert knowledge" into machine learning models.

We assembled a multidisciplinary consortium of experts in remote sensing, agriculture, artificial intelligence (AI), space operations, and hardware engineering. The central objective of the HYPERVIEW challenge was to advance the state of the art in soil parameter retrieval from hyperspectral data, especially in view of the Intuition-1 mission. Intuition-1 is a 6U-class satellite (Fig. 1) designed by KP Labs[1] to observe the Earth using a hyperspectral instrument and an on-board computing unit capable of processing data using AI. It is the world's first satellite with a processing power capable of advanced processing of HSIs in orbit—Intuition-1 was launched on November 11, 2023. Of note, the algorithms for soil parameter estimation are independent of the internals of Intuition-1 and can be deployed on board other satellites with hyperspectral sensors and AI capabilities. The winners of HYPERVIEW were awarded the unique opportunity to deploy their solutions aboard Intuition-1, hence contributing to advancing Earth observation. Eligibility for inclusion in the rankings was contingent upon participants delivering their implementations, with the rigorous verifiability and reproducibility of their submissions being unequivocally established.

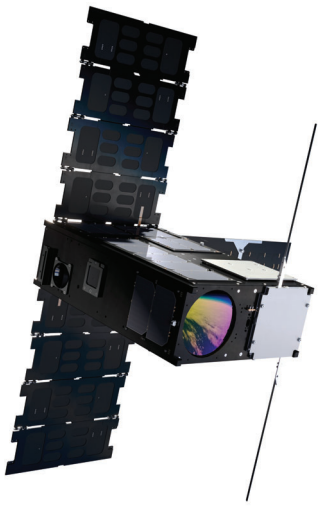

Fig. 1: Intuition-1 (credits: KP Labs, AAC Clyde Space).

We believe that our work will be an important step toward standardizing the way the community validates the emerging solutions in (not only) soil analysis from remotely-sensed HSIs. We hope that our dataset, alongside the current state-of-the-art results will become an exciting point of departure for further research in precision agriculture, ultimately bringing commercial and scientific value to the community.

B. Article Structure

In Section II, we present the details of the HYPERVIEW dataset and elaborate on the process of data acquisition, preprocessing, and designing the AI-ready datasets used in the challenge. It is discussed in Section III, where we present the validation procedure, and analyze the results of HYPERVIEW. Here, we deliver the organizers' insights concerning the progress of the challenge, dataset characteristics, and show

[1]KP Labs is a New Space company based in Poland, with the mission of accelerating space exploration by advancing autonomous spacecraft operation and robotic technology. For more details, see https://kplabs.space/.

how to assess the best-performing algorithms using other metrics commonly exploited in precision agriculture. Sections IV–VII summarize the top-ranked algorithms, providing the participants' perspective on HYPERVIEW. In the supplementary materials, we present the participants' strategies for verifying the algorithms during the challenge, when the quantitative results over the full test set were not revealed. Section VIII delivers the conclusions, summarizes the current state of the art in estimating soil parameters from the HYPERVIEW data, and highlights some interesting research pathways. In the supplementary materials, we include the co-authors' affiliations and roles, and a table of abbreviations used in this article.

II. HYPERVIEW: DATASET

On March 3, 2021, the data acquisition campaign was conducted, utilizing hyperspectral imagers mounted on the Piper PA-31 Navajo aircraft. It operated at an altitude of 2550 to 2700 meters, maintaining a cruising speed of 61.8 meters per second, and capturing imagery at a ground sampling distance (GSD) of 2 meters. The acquisition process was performed in the cloudless and windless weather. The acquisition system was founded upon HySpex VS-725 (Norsk Elektro Optikk AS), and comprised two SWIR-384 imagers and one VNIR-1800 imager, facilitating simultaneous data acquisition (Table I). Once the HSIs had been acquired on board the aircraft, the pre-processing routines were applied:

- **Radiometric calibration**. The raw spectral data are initially stored as discrete Digital Numbers (DNs), which are influenced by a complex interplay of factors, such as surface conditions, atmospheric effects, topographic influences, and sensor characteristics [78]. We radiometrically corrected such DN values to obtain the normalized values of DNs.
- **Geometric correction** was applied based on the Digital Surface Model (DSM) and flight parameters registered by the Global Positioning & Inertial Navigation System. The nearest neighbor technique was used for data resampling—it was done using PARGE (https://www.hyspex.com/hyspex-products/hyspex-processing-software/parge/, accessed on March 21, 2024).
- **Atmospheric correction** was performed using the moderate resolution atmospheric transmission technique [79], [80].
- **Mosaicing**—each of the hyperspectral mosaics consisted of hyperspectral series, with the horizontal overlay between them equal to 30% (or more). The bands below the 965 nm wavelength were captured by the HySpex VNIR-1800 sensor, whereas the bands above 965 nm were acquired by the HySpex SWIR-384 sensor. The resulting images are of 2 m GSD and encompass a total of 430 hyperspectral bands.

TABLE I: Characteristics of the imagers. For more details, see the supplementary materials.

Characteristics	SWIR-384	VNIR-1800
Spectral range [nm]	930–2500	400–1000
Spectral resolution [nm]	5.45	3.26
Number of bands	288	186

The in-situ measurements of the soil parameters were collected in August–November 2020, and the lab analysis was performed following the Mehlich 3 approach [81]–[83]. In our study, 12 soil samples were acquired for each field following the Zig-Zag pattern [84], and the fields varied in size, ranging from 0.5 to 4.0 hectares. Thus, for larger fields, the heterogeneity of collected soil samples may be inherently larger than for spatially smaller fields. As in other soil analysis studies [34], collected soil samples were mixed together and underwent the laboratory analysis which resulted in one tuple of four ground-truth values per each field (corresponding to one hyperspectral patch), containing phosphorus pentoxide (P_2O_5), potassium oxide (K_2O), magnesium (Mg), and the soil pH. Therefore, the HYPERVIEW dataset contains the hyperspectral patch-level ground-truth values for each soil parameter, where each hyperspectral patch corresponds to one field (the ground-truth values of specific pixels within the patch are thus unknown)—it might be considered a limitation of the dataset. Additionally, since the soil samples collected in each field are mixed together before the laboratory analysis, the information about their spatial locations within the field is lost. In Fig. 2, we show the pivotal steps of creating the dataset.

TABLE II: Descriptive statistics of the ground-truth soil parameters in the $\boldsymbol{T}$, $\boldsymbol{V}$, and Ψ sets.

Parameter	Subset	Min	Max	Average	Median
P_2O_5	$\boldsymbol{T}$	20.3	325.0	70.3	65.1
	$\boldsymbol{V}$	18.0	309.0	70.6	64.5
	Ψ	4.8	309.0	70.8	64.3
K_2O	$\boldsymbol{T}$	21.1	625.0	228.0	216.0
	$\boldsymbol{V}$	114.0	636.0	229.3	216.0
	Ψ	114.0	636.0	227.8	215.0
Mg	$\boldsymbol{T}$	26.8	400.0	159.3	155.0
	$\boldsymbol{V}$	61.9	410.0	161.6	155.0
	Ψ	61.9	410.0	160.6	156.0
pH	$\boldsymbol{T}$	5.6	7.8	6.8	6.8
	$\boldsymbol{V}$	5.9	7.9	6.8	6.8
	Ψ	5.5	7.9	6.8	6.8

The HYPERVIEW dataset includes 2886 hyperspectral patches, and each patch corresponds to exactly one field—see the examples in the supplementary materials. These patches never overlap and are spatially disjoint. The patch size varies (depending on the field), and it is around 60×60 pixels on average. Each patch contains 150 contiguous hyperspectral bands from the 462–942 nm spectral range (spectral resolution of 3.2 nm), reflecting the spectral range of the Intuition-1 sensor. All patches are split into 1732 training patches, constituting the training set $\boldsymbol{T}$, and 1154 test patches, being the test set Ψ. We extracted the validation set $\boldsymbol{V}$ from Ψ, containing 50% random test patches (thus, $\boldsymbol{V} \subset \Psi$). This validation set was used during the challenge to monitor the progress of the participating teams. To reduce the probability of over-fitting to Ψ, the participants were able to see their results obtained exclusively over $\boldsymbol{V}$ during the challenge. In Table II, we can see that the characteristics of the $\boldsymbol{T}$, $\boldsymbol{V}$ and Ψ are consistent, as they are all stratified according to the distributions of the ground-truth measurements of all soil parameters. This observation is confirmed in Figs. 3–5 which render the distribution of the ground-truth measurements, together with their cumulative distributions and histograms for $\boldsymbol{T}$, $\boldsymbol{V}$, and Ψ. Finally, the spatial coverage of the hyperspectral patches included in $\boldsymbol{T}$, $\boldsymbol{V}$, and Ψ amounts to 2220, 370, and 740 hectares. It makes the HYPERVIEW dataset—to our

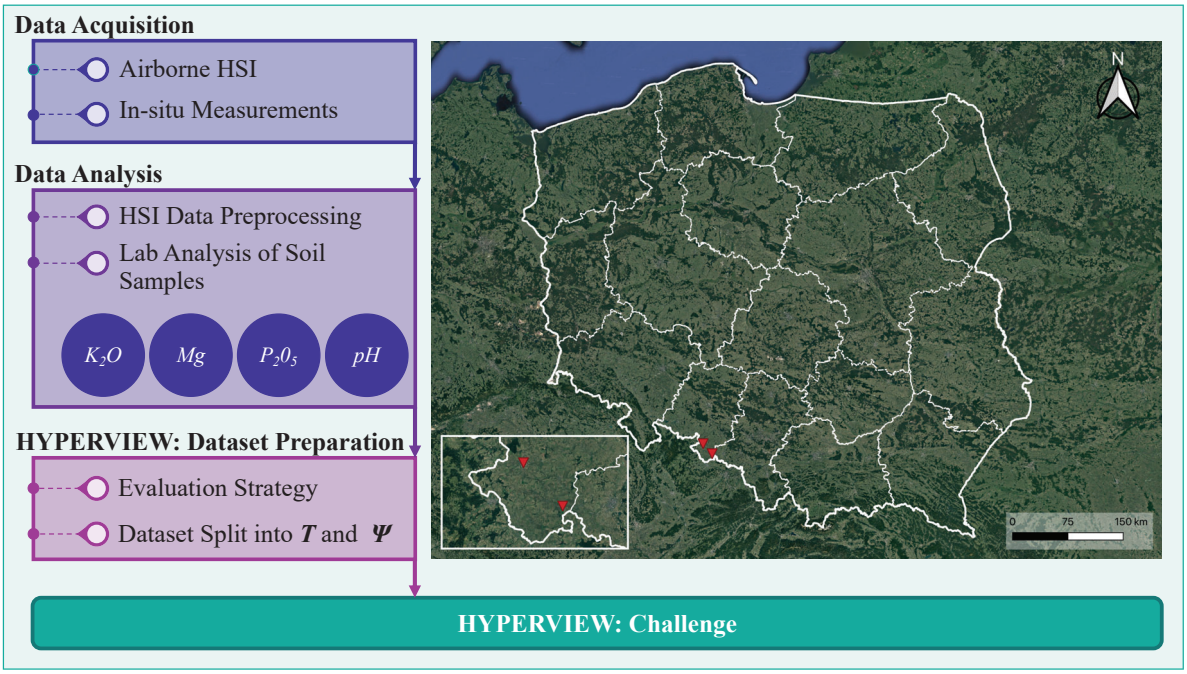

Fig. 2: The process of creating the HYPERVIEW dataset involved acquiring soil samples and airborne HSIs, performing the laboratory analysis of soil samples, and introducing the training-test split with the evaluation strategy to assess the algorithms.

knowledge—the largest dataset that could be used to validate data-driven algorithms for estimating soil parameters from HSIs.

III. HYPERVIEW: Challenge

Although the HYPERVIEW challenge has been already concluded [85], there is a permanently open version of HYPERVIEW available on the AI4EO platform: https://platform.ai4eo.eu/seeing-beyond-the-visible-permanent. Here, the HYPERVIEW dataset (split into the training and test subsets; note that the ground-truth data for the test set have never been revealed to the public) can be downloaded. Thus, anyone can push the state of the art in estimating soil parameters from HSIs through developing new algorithms and confronting them with the best solutions, as the up-to-date Leaderboard is available as well. To help participants get started with the challenge, we prepared a Jupyter Notebook (Starter Pack) to guide them through the data input/output operations, visualization, prediction using a baseline algorithm, and creating a valid submission. The Starter Pack is available through GitHub: https://github.com/AI4EO/kp-labs-seeing-beyond-visible-challenge.

A. Evaluation

1) Quality metric (HYPERVIEW Score): The quality score (dubbed the HYPERVIEW score) of each participating team, which quantifies their performance in the HYPERVIEW challenge, is computed through the following methodology:

$$\text{Score} = \frac{\sum_{i=1}^{4} \left(\text{MSE}_i / \text{MSE}_i^{\text{base}} \right)}{4}, \tag{1}$$

where the mean squared error for the i-*th* soil parameter is:

$$\text{MSE}_i = \frac{\sum_{j=1}^{|\Psi|} \left(p_{i,j} - \hat{p}_{i,j} \right)^2}{|\Psi|}, \tag{2}$$

and $|\Psi|$ is the cardinality of the test set (being the number of test patches), $p_{i,j}$ and $\hat{p}_{i,j}$ are the estimated and ground-truth soil parameters for the i-*th* soil parameter (P_2O_5, K_2O, Mg, or pH) in the j-*th* test patch. We calculate four mean squared error (MSE_i) values over the entire validation/test set ($\boldsymbol{V}$ or Ψ), one for each parameter (P_2O_5, K_2O, Mg, or pH), and divide them by the corresponding MSE value obtained using a "trivial" algorithm returning the average soil parameter from $\boldsymbol{T}$. **The lower scores denote the better solutions**, as they reflect predictions that closely align with the ground truth, with a quality score of zero representing a perfect match.

2) Illustrative example: Let us assume the following[2]:

- We have three competing algorithms: Algorithm A, Algorithm B, and Algorithm C. Each of them yields specific MSE values for all parameters (P_2O_5, K_2O, Mg, and pH).
- The baseline algorithm, which computes the average parameter value from $\boldsymbol{T}$, generates the following MSE scores over Ψ for P_2O_5, K_2O, Mg, and pH: 2500, 1100, 2000, and 3.

In Table III, we present the baseline MSE alongside the MSE values obtained by three algorithms A–C, and divided by the baseline MSE. The baseline MSE serves as a metric to evaluate the performance of an algorithm that simply calculates the average value for each parameter based on the data within the

[2]In order to ensure consistency with the HYPERVIEW documentation which was shared with the participating teams, the same illustrative example of the scoring methodology was given to the participants of the challenge [85].

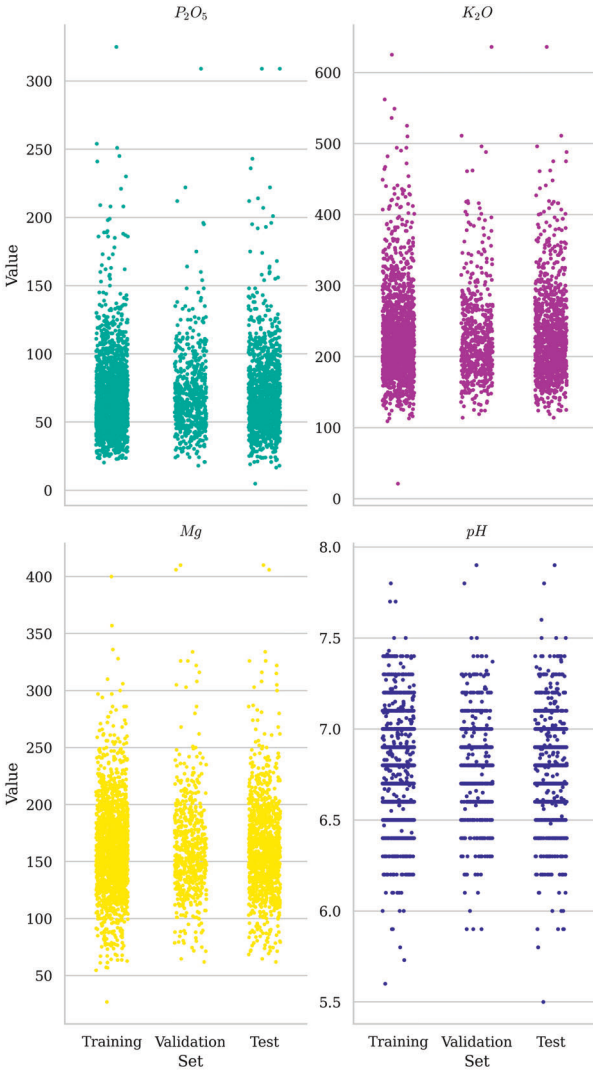

Fig. 3: The ground-truth measurements of all soil parameters in the $\boldsymbol{T}$, $\boldsymbol{V}$, and Ψ sets.

training set. The MSE values are subsequently used to compute the quality scores, which are further linked to the rankings (Table IV). It is important to emphasize that Algorithm B exhibits the most favorable performance, as it attains the lowest quality score. Algorithm B surpasses both Algorithm A and C, which is reflected in its superior ranking.

TABLE III: The baseline MSE, together with the MSE values obtained using three competing algorithms (Algorithm A–C). The best MSE and the best HYPERVIEW scores are **boldfaced**—the HYPERVIEW score amounts to 0.000 for Algorithm B for the pH estimation, meaning that it obtained the perfect predictions equal to the ground-truth pH values.

	MSE				$\text{MSE}/\text{MSE}^{\text{base}}$		
Parameter	**Baseline**	**Alg. A**	**Alg. B**	**Alg. C**	**Alg. A**	**Alg. B**	**Alg. C**
P_2O_5	1100	**500**	1000	1500	**0.455**	0.909	1.364
K_2O	2500	2000	2100	**100**	0.800	0.840	**0.040**
Mg	2000	1500	**100**	1700	0.750	**0.050**	0.850
pH	3	1	**0**	5	0.333	**0.000**	1.667

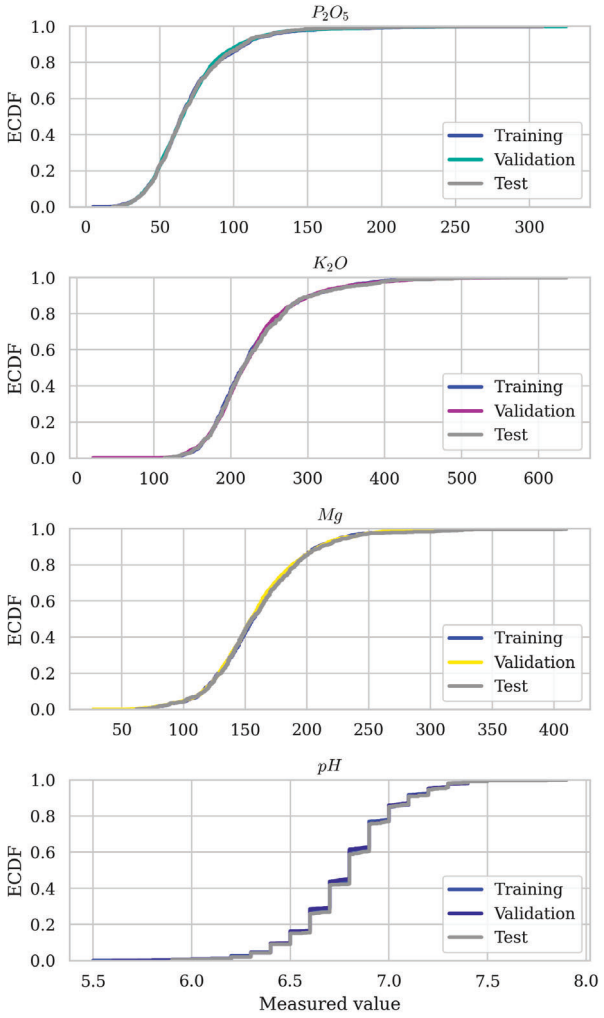

Fig. 4: Cumulative distribution function (ECDF) of the ground-truth measurements of all soil parameters in $\boldsymbol{T}$, $\boldsymbol{V}$, and Ψ.

TABLE IV: The aggregated HYPERVIEW score obtained for three soil parameter estimation algorithms A–C, alongside the corresponding ranking. Algorithm B is the winner (the smaller the score gets, the better algorithm is, as it returns the soil parameter values which are closer to the ground truth in-situ measurements). The best HYPERVIEW score is **boldfaced**.

Algorithm	**Score**	**Ranking**
Algorithm B	**0.450**	1
Algorithm A	0.584	2
Algorithm C	0.980	3

B. The Results

The live scoring tool was continuously evaluating the quality of the submitted solutions throughout the challenge—all valid submissions were ranked based on the HYPERVIEW score (Section III-A1). Each valid submission was required to include predictions for the soil parameters across all samples within Ψ. To maintain fairness and prevent potential server overload and undesirable practices like "sampling" the test data distribution, participating teams were allowed to upload their solutions at intervals of 12 hours. Furthermore,

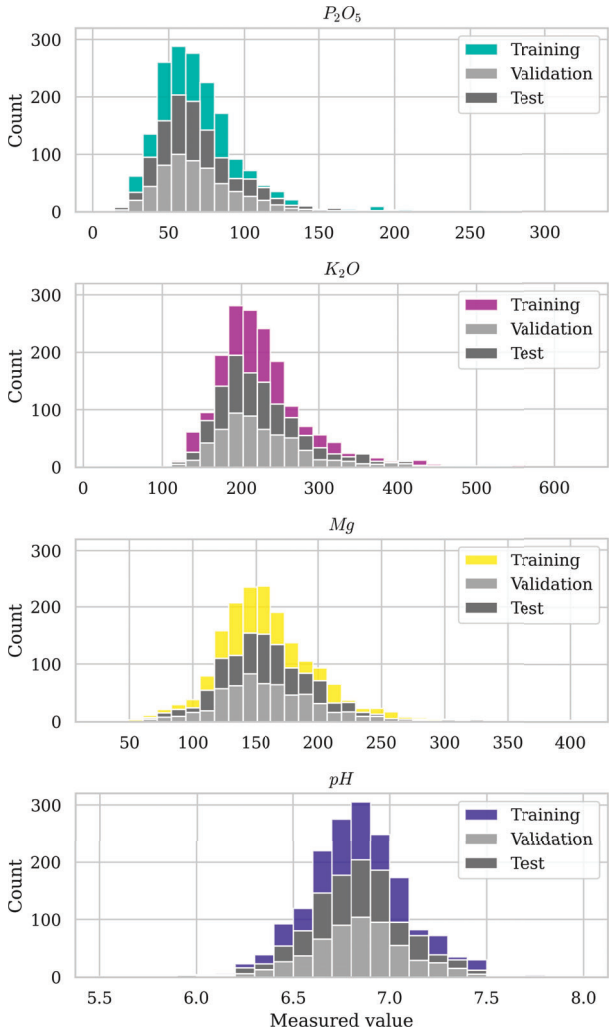

Fig. 5: The histograms of the ground-truth measurements of all soil parameters in the $\boldsymbol{T}$, $\boldsymbol{V}$, and Ψ sets.

to mitigate the risk of over-fitting to Ψ, participants had the opportunity to assess their quantitative results, specifically the aggregated HYPERVIEW score, which was obtained over $\boldsymbol{V}$, encompassing 50% of all test samples (see Section II). In this case, the MSE value obtained by the baseline ("trivial") solution returning the average value of each parameter (based on $\boldsymbol{T}$) was calculated for $\boldsymbol{V}$ as well. The HYPERVIEW scores achieved over $\boldsymbol{V}$ were displayed on the **Public Leaderboard**, providing participants with continuous visibility into their performance—its final layout is given in Table V. In total, the challenge garnered active participation from 46 teams, out of the 159 teams that had registered for the event. In Fig. 6, we can observe the distribution of the scores obtained over $\boldsymbol{V}$ by the top 25 teams. While there were outlier submissions for nearly all teams, this figure highlights the convergence of the top participants toward high-quality solutions which were finally fine-tuned (see the "clustered" scores on the left).

Once the challenge had finished, the final ranking was re-computed based on Ψ, including 1154 test examples, and the **Private Leaderboard** including the HYPERVIEW scores

TABLE V: The final status of the Public Leaderboard (i.e., the HYPERVIEW scores obtained for the validation set $\boldsymbol{V}$). The teams which submitted the Jupyter Notebooks for the final evaluation are **boldfaced** (those solutions which we were unable to successfully reproduce are underlined).

Rank	Team	Submissions#	Score
1	**EagleEyes**	67	0.781
2	**MOAH**	78	0.797
3	Black Cat	32	0.803
4	WEGIS	16	0.812
5	**Cap2AIScience**	45	0.816
6	Predictia	45	0.848
7	**deep_brain**	6	0.853
8	**u3s_lab**	31	0.871
9	**πK**	32	0.875
10	CMG	10	0.877
11	**rdeggau**	39	0.885
...			
15	jsoeo	10	0.909
...			
20	Hyper_Sense	4	0.945
...			
25	Tmw_geographer	9	0.977
...			
28	GU Orbit	7	0.989
...			
46	RandomAccess	6	2.119

obtained for Ψ was determined. This process could have led to changes in the final ranking, since the HYPERVIEW score on $\boldsymbol{V}$ may differ from the score on Ψ. In HYPERVIEW, we were devoted to combat the reproducibility crisis [77]. Thus, to be classified in the final ranking, the teams had to submit a Jupyter Notebook with the implementation to allow the organizers to reproduce the predictions. Out of 10 top-performing teams, seven teams submitted their implementations, and we were able to reproduce five of them (for πK, there were unresolved issues in the submitted Jupyter notebook, whereas deep_brain did not share their models with us, and we were unable to re-train them to obtain the HYPERVIEW scores similar to those calculated based on the submitted predictions). Finally, the top-4 teams (EagleEyes, MOAH, Cap2AIScience, and u3s_lab) decided to share the description of their approaches and related experimentation with us, hence they contributed to this manuscript.

TABLE VI: The HYPERVIEW scores obtained by the top-5 teams over $\boldsymbol{V}$ and Ψ, and calculated (*i*) by the server during the challenge (*Submitted*), and (*ii*) by the organizers using the models delivered by the participants (*Reproduced*). We report the difference (Δ) between the validation and test scores calculated by the organizers and by the server.

		Validation set ($\boldsymbol{V}$)			Test set (Ψ)		
Rank	Team	Submitted	Reproduced	Δ	Submitted	Reproduced	Δ
1	EagleEyes	0.781	0.788	−0.007	0.789	0.795	−0.006
2	MOAH	0.797	0.797	0.000	0.808	0.808	0.000
3	Cap2AIScience	0.816	0.817	−0.002	0.827	0.828	−0.001
4	u3s_lab	0.871	0.871	0.000	0.878	0.878	0.000
5	rdeggau	0.885	0.885	0.000	0.896	0.896	0.000

In Table VI, we gather the final HYPERVIEW scores. For all top-performing teams, we report the scores calculated over $\boldsymbol{V}$ and Ψ for the best submitted predictions (*Submitted*), and obtained through our reproducibility study based on the received Jupyter Notebooks (*Reproduced*)—the latter were used as the final scores for all participants. All of those techniques

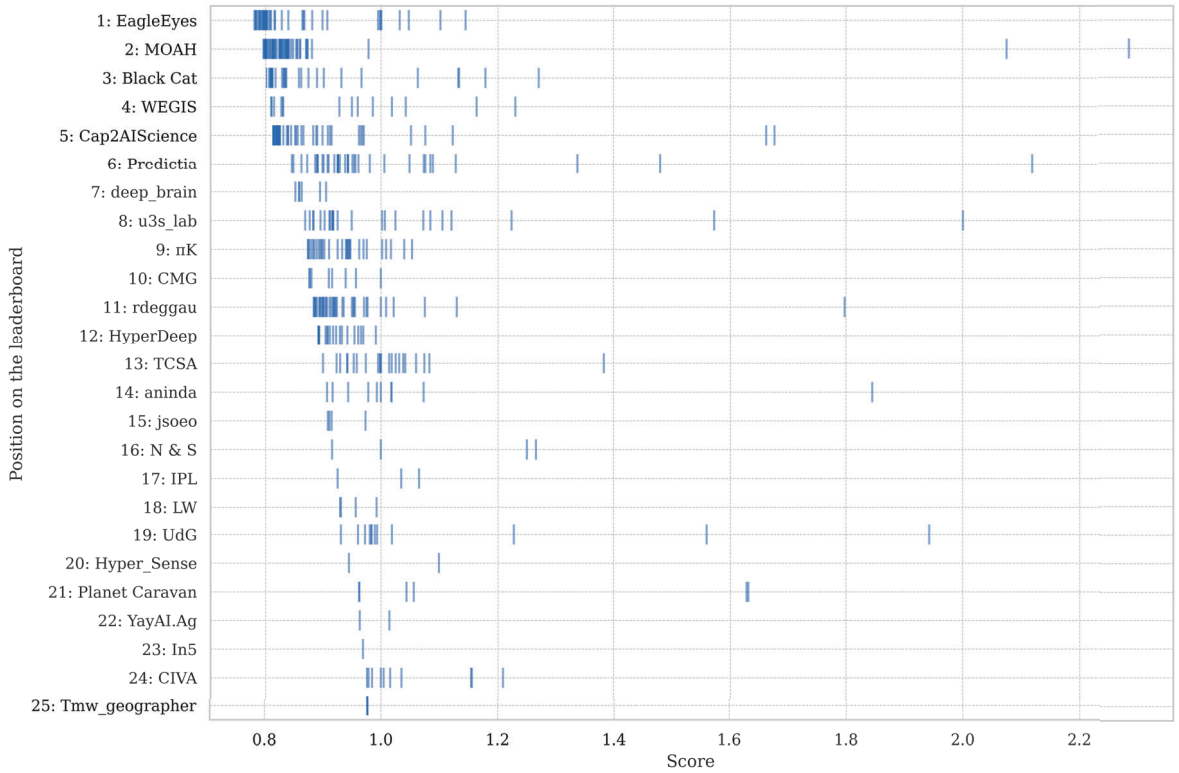

Fig. 6: The distribution of the HYPERVIEW scores for the top-25 teams (Public Leaderboard) participating in the challenge.

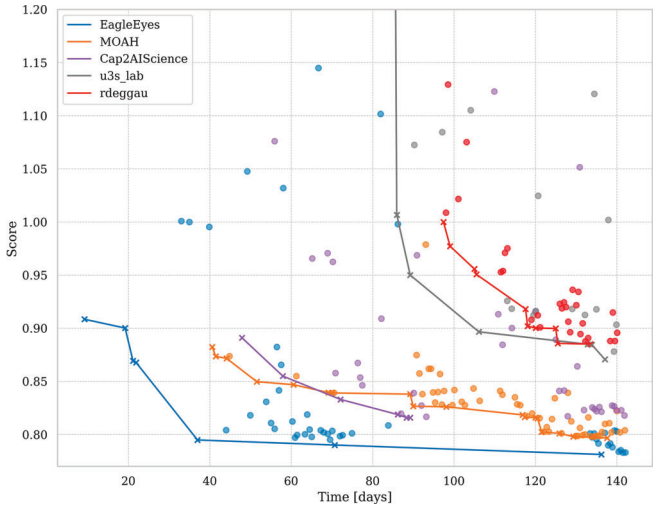

Fig. 7: The HYPERVIEW scores obtained by the top-5 teams during the challenge over the validation set $\boldsymbol{V}$.

are reproducible with rather minor differences between the submitted and reproduced predictions (Table VI). Those minor differences did not affect the final ranking. It is interesting to see Fig. 7, where we render the progress of the top-5 teams, quantified as the HYPERVIEW score calculated over $\boldsymbol{V}$. The winning team (EagleEyes) converged to their high-quality solutions relatively fast (in less than 40 days), and then they were subjected to fine-tuning. On the other hand, u3s_lab managed to improve their algorithm at the very end of the challenge. This progress plot (Fig. 7) was not visible to the participants, therefore they were unable to easily monitor that (unless they had implemented it themselves).

To investigate the quality of predictions of the top-5 teams, we show the Bland-Altman plots in Fig. 8, alongside additional metrics, with MSE, mean absolute error (MAE), mean absolute percentage error (MAPE), and coefficient of determination (R^2) commonly used in the soil analysis research:

$$\mathrm{MAE}_i = \frac{\sum_{j=1}^{|\Psi|} |p_{i,j} - \hat{p}_{i,j}|}{|\Psi|}, \tag{3}$$

$$\mathrm{MAPE}_i = \frac{100\%}{|\Psi|} \sum_{j=1}^{|\Psi|} \left| \frac{p_{i,j} - \hat{p}_{i,j}}{p_{i,j}} \right|, \tag{4}$$

and

$$\mathrm{R}^2{}_i = \frac{\sum_{j=1}^{|\Psi|} (p_{i,j} - \hat{p}_{i,j})^2}{\sum_{j=1}^{|\Psi|} (p_{i,j} - \bar{p}_i)^2}, \tag{5}$$

where $|\Psi|$ denotes the cardinality of the test set (the number of test patches), $p_{i,j}$ and $\hat{p}_{i,j}$ are the estimated and ground-truth soil parameter values for the i-*th* soil parameter (P_2O_5, K_2O, Mg, or pH) in the j-*th* test patch. Additionally, we calculate the relative mean absolute error (rMAE), which divides MAE of the algorithm by MAE of the baseline technique returning

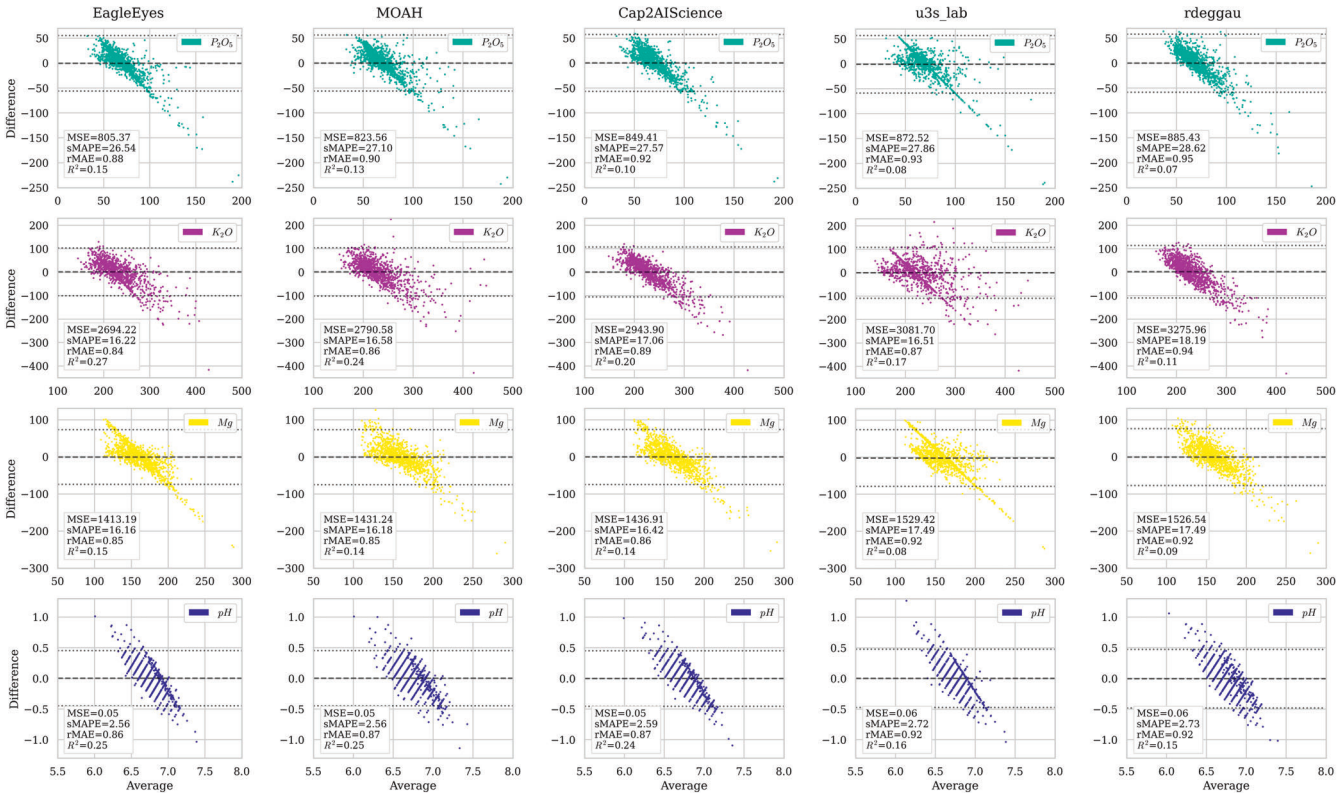

Fig. 8: Bland-Altman plots for the top-5 teams obtained over Ψ show the agreement between the predictions and ground truth.

the average of the i-*th* parameter value (p_i^{base}) based on $\boldsymbol{T}$:

$$\text{rMAE}_i = \frac{\sum_{j=1}^{|\Psi|} |p_{i,j} - \hat{p}_{i,j}|}{\sum_{j=1}^{|\Psi|} |p_{i,j} - p_i^{\text{base}}|}. \quad (6)$$

Also, we report the symmetric MAPE (sMAPE), being a modified version of MAPE, where the divisor is half of the sum of the ground truth and predicted i-th soil parameter [86]:

$$\text{sMAPE}_i = \frac{200\%}{|\Psi|} \sum_{j=1}^{|\Psi|} \frac{|p_{i,j} - \hat{p}_{i,j}|}{|p_{i,j}| + |\hat{p}_{i,j}|}. \quad (7)$$

The rMAE values indicate that all of the top teams outperformed the baseline, and all other measures consistently show that EagleEyes achieved the highest-quality predictions of all parameters. The shape of the Bland-Altman plots is similar for all top-performing methods—the largest errors are observed for large values of P_2O_5, K_2O, and Mg, as the patches corresponding to such parameters were under-represented in $\boldsymbol{T}$ (Fig. 3). An interesting distribution of the pH errors in Fig. 8 reflects the in-situ measurements of this parameter (Fig. 3).

The in-situ measurements were performed in the fields cultivated by three farmers (Farmer A, Farmer B, and Farmer C). They might be therefore cultivated differently, and the farmers might have followed a (slightly) different soil sampling procedure—albeit "standardized" across all farmers. In Fig. 9, we present the Bland-Altman plots rendering the EagleEyes's prediction errors for all parameters split across Farmers A–C. We can appreciate that the distribution of such errors significantly differs across those farmers, indicating the potential importance of developing specialized models not only for specific parameters, but also for land characteristics or cultivation approaches. This real-life data heterogeneity shows the difficulty of developing fully data-driven algorithms that are not benefiting from such additional "expert knowledge" that could be easily incorporated into the processing pipeline.

IV. First Place: EagleEyes

1) Data Preparation: Each hyperspectral patch corresponding to an agricultural field has a dimension of $w \times h \times \mathcal{B}$, where the width ($w$) and height ($h$) are variable, but the number of bands ($\mathcal{B}$) remains constant (150) for all patches. Thus, the data corresponds to the reflectance per pixel and wavelength. The distribution of patch sizes is skewed—approximately one-third of them have a size of 11×11 pixels, and 60% of the patches have a width or height of fewer than 50 pixels (Fig. 10). Patches with a spatial size of 11×11 or smaller are referred to as *small patches*, and the rest as *large patches* in our experiments. Based on this distinction, different feature extraction and machine learning techniques are used.

2) Feature Extraction and Augmentation for Classical ML: When extracting features for classical ML (Fig. 12a), the aim is to include attributes from the whole patch while keeping as much of the physical relations in the patch as possible. The presence of certain chemical elements can be determined through their distinct spectra, and it is therefore assumed that the concentration of soil parameters K_2O, P_2O_5, and Mg could be inferred from the spectra. Furthermore, the spectra

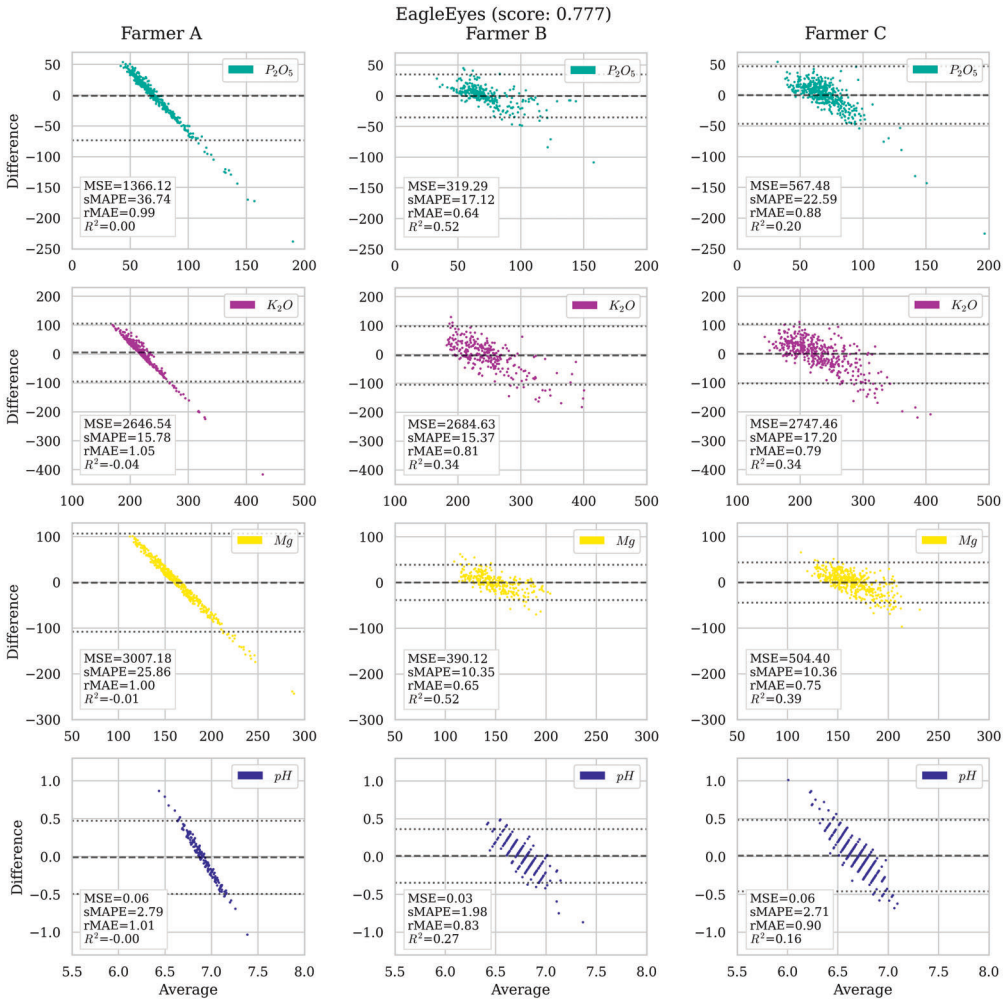

Fig. 9: Bland-Altman plots for the EagleEyes team obtained over three subsets of Ψ (the fields cultivated by Farmer A, Farmer B, and Farmer C) show the agreement between the predictions and ground truth.

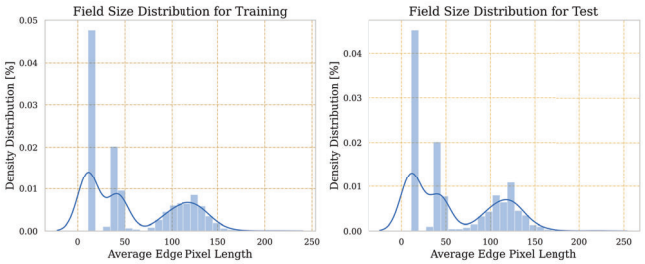

Fig. 10: **EagleEyes:** Distribution of patch sizes.

of other compounds can be dependent on the local pH value. To account for the varying patch size, the average reflectance is calculated for all pixels in the patch per wavelength (Fig. 11). Note that the spectra vary visually for different targets, which would hopefully be leveraged during the ML process.

From the average reflectance, further features are derived:

- The gradient of the average reflectance up to the 3^{rd} order,
- The wavelet transform of the average reflectance up to the 4^{th} level of approximation and detail coefficients,
- The real and imaginary parts of the Fast Fourier Transform (FFT) extracted from the average reflectance.

Features are also extracted through Singular Value Decomposition (SVD) of each band (b) in a patch ($\mathcal{P}$), such that $\mathcal{P}_{(w\times h\times b_i)} = U_i\Sigma_i V_i^T$, where $i \in \{1, 2, \ldots, 150\}$ is the index of band (b). Therefore, we extract:

- The first 5 diagonal values, σ_j, where $j \in \{1, 2, \ldots, 5\}$, for each Σ_i matrix of size $[r \times r]$, where $r \leq \min\{w, h\}$,
- The ratio of the two diagonal values σ_1/σ_2 of each Σ_i,
- The real and imaginary parts of the FFT extracted from the ratio array (σ_1/σ_2 of each Σ_i).

With all features combined, an 1×2400 dimensional array for each patch is retrieved. Since the HYPERVIEW dataset size is limited, data augmentation is applied by randomly cropping the *large patches* into *small patches*, as well as by adding 1% Gaussian noise to the patches.

3) Data Handling and Augmentation for Deep Learning: When using deep learning (DL) models, the patches with the dimensions of $w \times h \times 150$ are directly fed into the prediction process. However, since the model requires a fixed width and height for each input, they are resized to 224×224 patches. To avoid over-fitting, training-time data augmentation techniques,

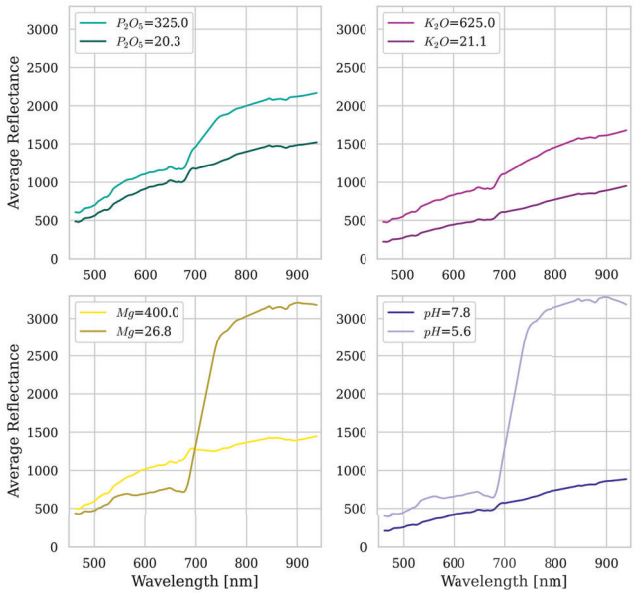

Fig. 11: **EagleEyes:** Average reflectance for different fields having the extreme target values for soil parameters.

such as adding Gaussian noise, random rotations, resizing and cropping, flipping, shifting, and scaling are applied in sequence with a 50% probability to the patches.

4) Classical and Deep Machine Learning Models: During the development process, various classical ML and DL methods were investigated [88]. We focus on two approaches:

1) *The hybrid ML model* based on the Random Forest (RF) and the K-nearest Neighbors (KNN) regressors, which produced the final winning score in HYPERVIEW,
2) The ViT-L/14 Vision Transformer deep learning architecture [89], where L stands for "large", and 14 refers to the number of layers in the network. In the ViT-L/14 architecture, an image is split into smaller patches, which are then flattened and treated as individual tokens (Fig. 12b). They are then passed through a sequence of self-attention and feed-forward layers. In our implementation, the evaluation metrics of ViT-L/14 were only slightly worse than those of the hybrid ML model.

The combined RF+KNN model is a more lightweight solution than ViT-L/14, which is beneficial in the context of this competition (i.e., the algorithm should be possible to run on board Intuition-1). However, ViT-L/14 has a greater potential for further improvement with larger datasets [90].

5) Code Availability: The implementation is available at: https://github.com/ridvansalihkuzu/hyperview_eagleeyes.

V. Second Place: MOAH

1) Data Preparation: The HYPERVIEW patches contain the spectral signature of soil which is influenced by properties such as mineral concentration, nutrition, and organic content [91]. To identify nutrient-sensitive wavelengths where reflectance is more correlated with a nutrient level, Pearson's correlation coefficients were used [92]. Linear correlation analysis was performed to assess the relationship between hyperspectral data and soil parameters. It helped determine the bands that are strongly correlated with specific parameters.

The results of linear correlation analysis between spectral reflectance and soil parameters indicate a sudden change in the correlation coefficient when moving from the visible to the near-infrared regions (Fig. 13a). There is a negative change for P_2O_5 and K_2O, while pH and Mg show a positive change. However, all parameters display a stable pattern of correlation in the near-infrared region. The analysis demonstrated that the parameters are correlated differently with spectral reflectance, with Mg exhibiting the highest correlation throughout the entire spectral range. Conversely, K_2O displays the lowest correlation across the spectrum, with the correlation close to 0. On the other hand, P_2O_5 has the highest inverse relation with spectral reflectance. This finding suggests that spectral reflectance responds differently to soil parameters, and modeling each parameter separately is more effective than using a single multi-task model for all four parameters.

The availability of nutrients in the soil can have an impact on the concentration of other parameters. Soil pH influences the availability of other nutrients [93]. The level of nitrogen can impact the pH and P_2O_5 levels based on various factors [94]. As a result, it is important to examine the relationship between the parameters in the study area to determine how they are correlated, and to analyze their distribution.

Not all target soil parameters are normally distributed, as shown in Fig. 13b, where P_2O_5 and K_2O exhibit a high skewness of 2.08 and 1.57, respectively. This makes it challenging for the model to make accurate predictions at the extreme ends of the distribution, and random sampling for cross-validation would result in unreliable evaluation. While the log or Box-Cox transformations are often employed to obtain normally distributed data, they can make the results harder to interpret, and this property is not desirable. Thus, the raw values of each soil parameter were discretized individually into 10 bins, and a stratified 10-fold technique was used to divide each bin. This approach is crucial to reliably evaluate the model's performance on a representative dataset with similar distribution while building a ML model.

The correlation matrix in Table VII was used to examine the relationship between the soil parameters. As expected, the parameters displayed varying degrees of correlation with each other. Notably, K_2O showed a positive correlation with P_2O_5, Mg, and pH, with correlation coefficients of 0.38, 0.25, and 0.13, respectively. On the other hand, the negative correlation coefficient of -0.15 between P_2O_5 and Mg indicates an inverse relationship between them. To improve the prediction results, a post-processing step was carried out on the model's outcomes, and this will be explained in the modeling section.

TABLE VII: **MOAH:** Correlation between the soil parameters.

	K_2O	Mg	pH
P_2O_5	0.38	-0.15	0.14
K_2O		0.25	0.13
Mg			-0.01

In the previous studies, researchers used specific wavelengths highly correlated with nutrient concentration to develop new vegetation indices to predict their concentration in

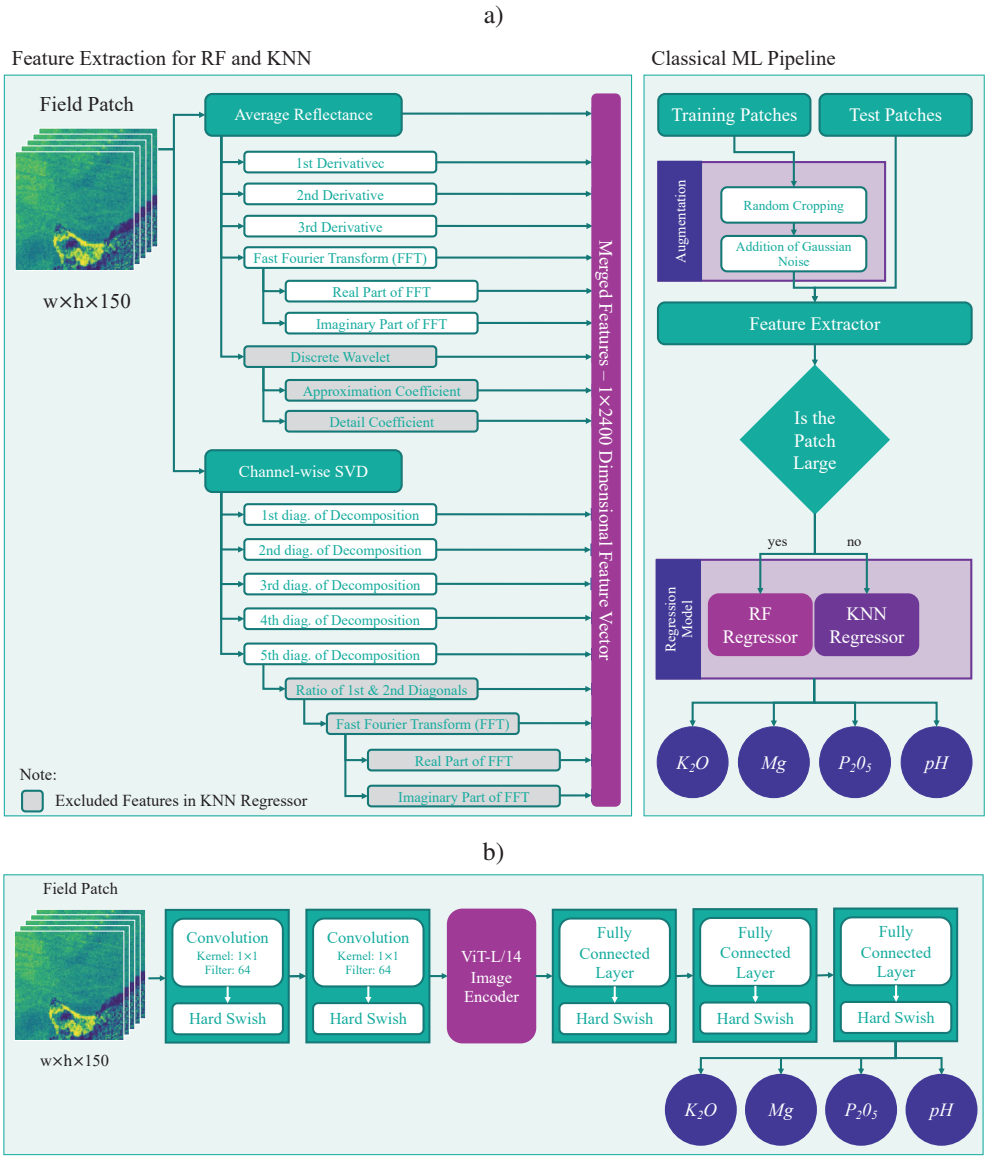

Fig. 12: **EagleEyes:** The a) detailed view of the feature extractor (left), and the prediction pipeline based on the classical ML (right), together with b) the ViT-L/14 prediction pipeline—the *Image Encoder* and its pre-trained weights were taken from [87].

soil [92]. Similarly, narrow-band indices (NBIs) were computed by exploring all possible band combinations to predict the vegetation cover [95]. However, in our case, we have a wide spectrum with a high spectral resolution, and using all possible indices in addition to different statistics like mean, median, minimum, maximum, and standard deviation for each band can lead to issues such as feature redundancy and overfitting, especially given a limited number of training samples. To address this challenge, Recursive Feature Elimination (RFE) was applied to Random Forests (RFs) with 100 trees, to select the top 500 features, with feature importance computed based on mean decrease impurity. RF was chosen as it does not require any prior steps to be performed on the data and is computationally efficient and faster than other models [95].

To help the models capture the highly nonlinear interactions, new features were added to the picked ones. The interactions between the top 10 selected features were computed and added to the feature set. As suggested by [96], pre-processing of the spectrum can improve results. Therefore, the second derivative of the spectral curve was supplemented to the best hand-crafted features of K_2O and P_2O_5 to create the final feature set. Fig. 14a gives an overview of generating the feature set.

2) Machine Learning Models: Ensemble tree-based models were used to predict soil parameters. Random Forests, CatBoost [97], Light Gradient Boosting Machine (LightGBM) [98], Extreme Gradient Boosting (XGB), and Extra Trees (all with default parameterization) were selected due to their interpretability, computational efficiency, and ability to handle unnormalized data [99]. Ensemble techniques are widely used to improve model performance and yield stable results. However, finding the optimal way to combine models remains an open challenge. In [100], forward stepwise selec-

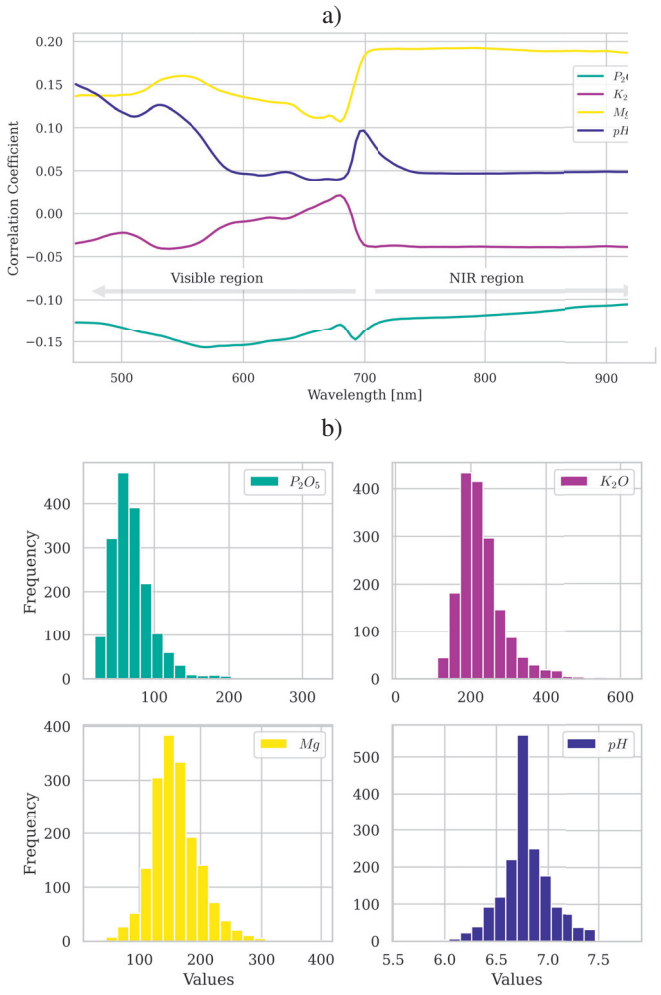

Fig. 13: **MOAH:** The a) linear correlation analysis (Pearson's correlation) between spectral reflectance and soil parameters, and b) distribution of soil parameters in the training set. *Note that the soil parameter values are binned differently than in Fig. 5, thus the minor differences in those histograms.*

tion was used from a large library of models, starting with an empty ensemble and adding the model that improved the performance, according to a selected metric, on a validation set. This approach assumes that the best ML models for the validation set will also be well generalizing over the test set. Under the assumption that the best model on the validation set would also perform best on the test set, different weights were assigned to the models based on their performance on the validation set for each fold. The following steps were performed to select the best weights for each model (Fig. 14b):

- **Step 1:** Trained ML models were used to obtain the predictions over the validation set, resulting in five prediction sets for each soil parameter (obtained using five models).
- **Step 2:** Random weights, summed to 1, were initialized.
- **Step 3:** The weights were assigned to the prediction results randomly, and a weighted sum was used to produce the final weighted prediction result.

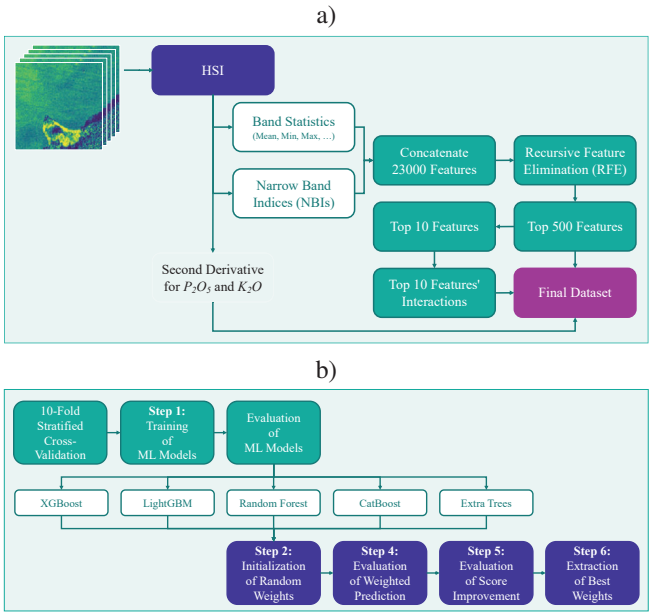

Fig. 14: **MOAH:** The a) workflow of generating the final feature set, and b) selecting the best model's weights.

- **Step 4:** The evaluation score was computed on the weighted prediction result, providing the first score to serve as a reference.
- **Step 5: Steps 2–4** were repeated for a specified number of iterations (in this case, 5000), and the score was checked each time to see if it had improved compared to the previously computed score.
- **Step 6:** The best weights that achieved the maximum performance on the validation set were returned.

The trained ML models and the best-selected weights were used to adjust the predicted soil parameters. This process was repeated for each of the 10 folds, resulting in 10 weighted predictions. To smooth out fluctuations in the predictions, the geometric mean was used to ensemble the predictions.

Post-processing was applied to improve the predictions by exploiting the correlations between the soil parameters. As discussed earlier, the parameters are interdependent and affect each other. To account for this, the predicted soil parameters were used as input data to predict themselves using Generalized Additive Models (GAMs) [101]. The following steps outline the post-processing method used for K_2O predictions (which was applied analogously to the other parameters):

- **Step 1:** The trained ML models were used to predict the soil parameters on the training set.
- **Step 2:** Predictions were adjusted using the best weights.
- **Step 3:** A GAM was trained using the predicted values of Mg, P_2O_5, and pH, with the goal of predicting the original K_2O values more accurately.
- **Step 4:** The trained GAM was used to predict K_2O, using the ensemble test predictions of Mg, P_2O_5, and pH.
- **Step 5: Steps 2–4** were repeated for the 10-fold cross-validation to generate ten sets of predictions.
- **Step 6:** The final prediction was obtained by taking the

geometric mean of ten prediction results.

3) Code Availability: The implementation is available at: https://github.com/masawdah/HYPERVIEW_MOAH.

VI. Third Place: Cap2AIScience

1) Data Preparation: In the exploratory analysis, Pearson's correlation coefficients between the four soil parameters with each wavelength were analyzed to verify if these parameters have specific absorption bands. We observed that the correlations were all close to zero for each parameter, hence we inferred that there is no correlation between the soil parameters and specific bands. Since there is only one value of each soil parameter per patch $\mathcal{P}$, but sometimes more than 10,000 pixels per patch and the number of training patches is limited, we need to tackle the challenges inherently related to such highly-dimensional data. To keep a single hyperspectral value per patch, the mean and the median of all pixels in each patch were calculated (the better performing transformation was later selected based on the model's performance).

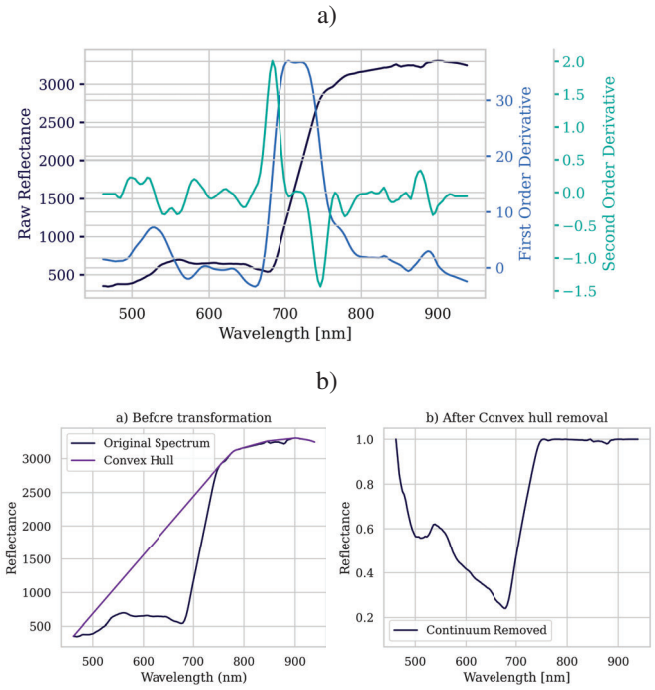

Fig. 15: **Cap2AIScience:** The a) derivatives of the spectral curves, and b) the continuum removal technique.

When using ML models over a hyperspectral spectrum, the information about its shape can be lost as the models can exploit each wavelength separately. To retain the shape information of the spectrum, the 1^{st} and the 2^{nd} derivative over the mean and median spectral curves were added to the input [70], [102], [103] (Fig. 15a). We considered two methods to normalize the HSI: (*i*) a global normalization by the full spectrum, and (*ii*) a normalization by a spectral band. The continuum removal technique was also used to normalize the spectra. A convex envelope, created using the convex hull, is fitted to the spectrum, and then the spectrum is divided by the convex envelope (Fig. 15b) [103]. Wavelet transformation and FFT were applied on the spectrum to extract the signal information [102]. Finally, the normalization and spectral transformation techniques offering the best soil parameters' estimation (according to our experiments) were retained. Also, we calculate NDVI to capture the details about the vegetation condition. An NDVI value close to one indicates a patch with vegetation, whereas when it is close to zero, the patch is "dry". It was used to verify if our models are sensitive to the vegetation. To reduce the feature vectors, potentially containing redundant features, we exploit Principal Component Analysis (PCA) and Independent Component Analysis on the spectrum and on each of its transformations.

2) Machine Learning Models: In Fig. 16, we render a flowchart of our ML pipeline for estimating the soil parameters. According to [102], and [70], Random Forests, Lasso Regression and Gradient Boosting Decision Trees can effectively retrieve soil parameters. The recent advances in deep learning might be used in this context as well [104], but we believe that deploying them on the satellite could be more challenging, hence we focused on the former techniques.

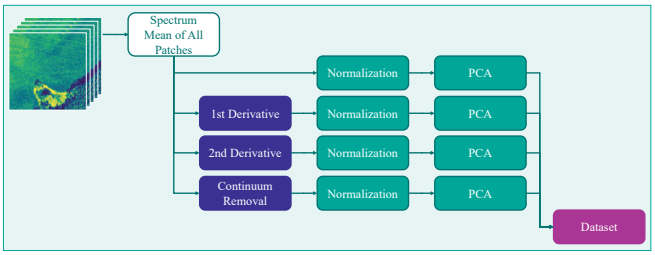

Fig. 16: **Cap2AIScience:** Flowchart of our ML pipeline.

VII. Fourth Place: u3s_lab

A. Method

1) Data Preparation: The patch size in the HYPERVIEW dataset is not uniform and varies in both height and width, with dimensions ranging from a minimum of 11 to a maximum of 284 pixels. Once the pixel values outside the region of interest (annotated by the available masks) are set to 0, a series of pre-processing and augmentation steps are implemented (Fig. 17):

- **Normalization.** The patches are normalized by dividing them by the maximum pixel value of the entire dataset. The same normalization is applied to the ground truth data, except for the pH parameter which is divided by 14, being the highest physically attainable value.
- **Tiling.** To match the input size of the Deep Neural Network (DNN) used in our study, small patches are replicated and stitched together in both directions. Any remaining size difference is addressed either through resizing or zero padding. In case the patch size exceeds the DNN input shape in both height and width, the patch is accordingly downsampled via bilinear interpolation. This method allows to train and test the network on consistent input shapes, despite the large variability in the dataset. Although some of the pre-processed images

consist of repeated patches, the ground truth labels are not impacted since they refer to the concentration values.
- **Flipping.** Tiling is coupled with random flips of the patches and the resulting image, to diversify the dataset.
- **Noise.** Gaussian noise with zero mean and 0.05 standard deviation is added to all hyperspectral bands.

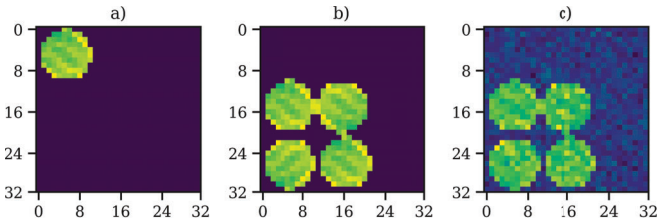

Fig. 17: **u3s_lab:** Image pre-processing: a) a single patch, b) tiled patch with random flips, c) addition of Gaussian noise.

2) Machine Learning Model: The model used to estimate the soil parameters is built upon the EfficientNet-LiteB0 network [105], which is a lightweight version of the EfficientNet architecture [106]. This choice was motivated by the need for the model to be energy and resource efficient. In this regard, the effortless scalability of the EfficientNet family and its reliance on 2D convolutions made it a good compromise for this application. Although 3D convolutions are more effective in extracting spectral-spatial features [107], they entail a higher computational cost. To adapt the network to the specific task, the input size is set to $32 \times 32 \times 150$ and a single layer dense regression head is attached to the latest feature map. Given the reduced input size, the original network is also scaled by half in both its width and depth, further reducing the computational burden, resulting in only about 734 thousand parameters. A visualization of the architecture obtained by using the Visualkeras [108] Python package is presented in Fig. 18. The model was trained for 300 epochs with a batch size of 32. An initial learning rate of $5{\cdot}10^{-3}$ was progressively reduced with a cosine decay law after a warm-up epoch starting at 10^{-3}. The Adam optimizer was employed along with MSE as a loss function.

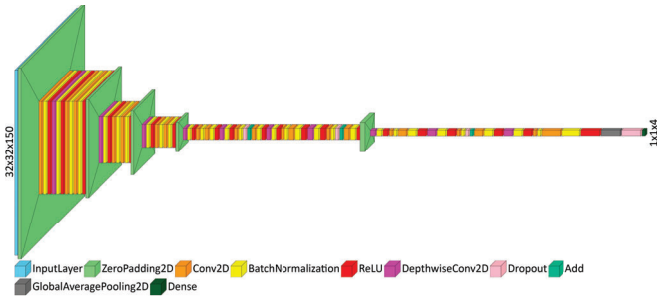

Fig. 18: **u3s_lab:** EfficientNetLiteB0mod: The DNN architecture of the regression model obtained by scaling and adapting the lite version of the EfficientNetB0 architecture.

3) Code Availability: The implementation is available at: https://github.com/Microsatellites-and-Space-Microsystems/hyperspectral-cnn-soil-estimation.

VIII. Concluding Remarks and Aftermath

Maintaining the sustainability of farms by enhancing agricultural management practices through the integration of recent advancements in Earth observation and artificial intelligence has emerged as a critical concern in contemporary agriculture. This approach serves a dual purpose: enabling farmers to tackle the challenge of cost-effective food production while promoting environmentally friendly agricultural practices. Farmers require timely access to information regarding soil parameters to optimize their fertilization processes. This optimization can lead to the selection of more suitable fertilizer blends and a reduction in overall fertilizer consumption.

The conventional method for quantifying soil parameters is labor-intensive and time-consuming. It involves collecting soil samples in the field, combining them, and sending them to specialized laboratories for chemical analysis. Moreover, the limited number of sampling points compromises the accuracy of the test results. In essence, this in-situ analysis is neither scalable nor efficient. However, there are alternative approaches that aim to automate the estimation of various soil parameters using hyperspectral imagery, offering non-invasive and scalable solutions. These algorithms are often validated across different datasets and training-test dataset splits, making direct comparisons difficult or even impossible.

We have addressed the existing research gaps related to the absence of standardized procedures that would enable unbiased validation of AI-driven algorithms designed to estimate soil parameters from real-life HSIs. Our approach involved the collection of airborne HSIs alongside ground-truth in-situ measurements. Then, we organized the HYPERVIEW challenge, which introduced a validation procedure for evaluating algorithms in this context. The HYPERVIEW challenge commenced on February 9, 2022, and concluded on July 1, 2022. This event garnered significant interest, with 159 registered teams, 46 of which actively participated by submitting their solutions to the evaluation server. Following an extensive final validation stage, where we meticulously replicated the top-performing approaches, we derived quality metrics for these algorithms. The outcomes (Table VIII) now represent the current state of the art of estimating key parameters such as phosphorus pentoxide (P_2O_5), potassium oxide (K_2O), magnesium (Mg), and soil pH over the HYPERVIEW dataset.

We encourage researchers to consistently exploit the metrics reported in Table VIII in their forthcoming studies that employ this dataset, as this practice will ensure a fair and objective basis for comparing different methodologies. To encourage widespread adoption of this approach within the scientific community, we have re-opened the HYPERVIEW challenge which is now permanently-open, and established an evaluation server at https://platform.ai4eo.eu/seeing-beyond-the-visible-permanent. Here, interested parties can freely access the HYPERVIEW data, along with a minimal example illustrating how to construct a model. Participants can then submit their predictions and track their quantitative metrics. We believe that our efforts represent a significant step toward the establishment of unbiased and objective validation procedures for evaluating emerging techniques aimed

TABLE VIII: The current state of the art of estimating soil parameters from HSIs over the HYPERVIEW test set (Ψ). For each metric, we indicate if it should be minimized (↓) or maximized (↑). We also report the metrics obtained by the baseline algorithm, returning the average value for each soil parameter calculated for the training set $\boldsymbol{T}$. The best results are **boldfaced**.

Parameter	Algorithm	MSE (↓)	MAE (↓)	rMAE (↓)	MAPE (↓)	sMAPE (↓)	R^2 (↑)
P_2O_5	EagleEyes	**805.374**	**19.064**	**0.881**	**31.305**	**26.542**	**0.151**
P_2O_5	MOAH	823.559	19.478	0.900	32.205	27.103	0.132
P_2O_5	Cap2AIScience	849.408	19.928	0.921	33.062	27.568	0.104
P_2O_5	u3s_lab	872.519	20.072	0.927	32.437	27.860	0.080
P_2O_5	rdeggau	885.430	20.667	0.955	34.192	28.622	0.066
P_2O_5	Baseline	948.452	21.649	1.000	36.053	30.070	0.000
K_2O	EagleEyes	**2694.217**	**37.829**	**0.841**	**16.889**	**16.220**	**0.271**
K_2O	MOAH	2790.577	38.633	0.858	17.416	16.579	0.245
K_2O	Cap2AIScience	2943.895	39.855	0.885	17.732	17.064	0.203
K_2O	u3s_lab	3081.704	39.035	0.867	17.092	16.514	0.166
K_2O	rdeggau	3275.961	42.517	0.944	19.130	18.190	0.113
K_2O	Baseline	3694.691	45.017	1.000	20.011	19.272	0.000
Mg	EagleEyes	**1413.191**	**25.949**	**0.851**	**17.539**	**16.156**	**0.153**
Mg	MOAH	1431.236	26.032	0.854	17.578	16.179	0.142
Mg	Cap2AIScience	1436.909	26.354	0.864	17.893	16.417	0.139
Mg	u3s_lab	1529.418	28.007	0.918	18.723	17.494	0.083
Mg	rdeggau	1526.539	28.058	0.920	18.882	17.489	0.085
Mg	Baseline	1668.651	30.500	1.000	20.570	19.034	0.000
pH	EagleEyes	**0.053**	**0.174**	**0.864**	**2.568**	**2.561**	0.246
pH	MOAH	**0.053**	**0.174**	0.866	2.571	2.564	**0.248**
pH	Cap2AIScience	**0.053**	0.175	0.873	2.591	2.586	0.241
pH	u3s_lab	0.059	0.184	0.916	2.724	2.715	0.156
pH	rdeggau	0.059	0.185	0.922	2.736	2.731	0.152
pH	Baseline	0.070	0.201	1.000	2.973	2.963	0.000

at estimating various parameters, including soil properties, from remotely-sensed data. It is of note, however, that the HYPERVIEW dataset can be further expanded to include additional soil properties [109]–[113] which can influence the agricultural management processes. We hope that our efforts will be a step toward building a wider set of well-established soil analysis benchmarks, coupling in-situ measurements with image data (and potentially other data modalities) that will be used to verify data-driven algorithms, with the ultimate goal of enhancing the current agricultural procedures.

Satellite imaging coupled with on-board data processing presents intriguing opportunities in the field of Earth observation, offering extensive scalability across vast geographical regions. Nevertheless, the transmission of large quantities of hyperspectral imagery from a satellite to Earth is impractical due to its time and cost inefficiency. The introduction of on-board AI holds the potential to significantly reduce the volume of data that needs to be transmitted. This, in turn, allows the global community to access valuable insights extracted from raw images more rapidly compared to conventional ground-based analysis methods. Ultimately, this approach paves the way for groundbreaking advancements in AI-powered Earth observation [114]. Therefore, one of our current objectives is to implement AI directly on board such edge devices. Our research was centered on a comprehensive evaluation of machine learning algorithms intended for deployment on board Intuition-1 [115], [116], with the bare soil detection and soil analysis built upon the results of the HYPERVIEW challenge being its first real-world downstream application.

After concluding the challenge, we have been observing various papers referring to the HYPERVIEW challenge and dataset, further underpinning their importance. We can split the emerging works into two groups (as of March 17, 2024):

- **Referring to the HYPERVIEW challenge and dataset** to show the advancements in the field of soil parameters' estimation, discuss the available datasets, and to show the importance of this research area: [114], [117]–[124].
- **Using the HYPERVIEW dataset** in the emerging research activities (to build new algorithms): [125]–[129].

The HYPERVIEW adoption is also reflected in the projects which exploit the HYPERVIEW dataset, such as those supported by the European Space Agency: "*Explainable AI for hyperspectral image analysis*" (PINEAPPLE) implemented by KP Labs (Poland) and Warsaw University of Technology (Poland) (years of implementation: 2023–2025), "*Fostering Advancements in Foundation Models via Unsupervised and Self-supervised Learning for Downstream Tasks in Earth Observation*" (FAST-EO) by German Aerospace Center (Germany), IBM Research (Switzerland), Forschungszentrum Jülich (Germany), and KP Labs (Poland) (2024–2025), and "*Weakly Supervised Learning for Hyperspectral Image Analysis*" by KP Labs (Poland) (2023–2024). Based on the current research interest, we believe that HYPERVIEW may pave the way to developing large-scale and thoroughly validated soil analysis solutions built upon Earth observation technologies.

ACKNOWLEDGMENT

This work was funded by European Space Agency (ESA), partly via a feasibility study for CHIME mission, and via Intuition-1 focused GENESIS project supported by Φ-lab (https://philab.esa.int/). JN, LT, AMW, and MK were supported by the Silesian University of Technology grant for maintaining and developing research potential.

EagleEyes: We thank Kai Konen, Roshni Kamath, and Lichao Mou for helpful discussions. This work was supported by the Helmholtz Association's Initiative and Networking Fund through Helmholtz AI [grant number: ZT-I-PF-5-01] and on the HAICORE@FZJ partition.

Cap2AIScience: Capgemini's Science&AI team is a pool of experts with varied and complementary skills. The challenge

was accomplished thanks to our internal R&D capacity. A team of physicists and data scientists were implicated in the realization. We want to thank all the Capgemini team involved: ANGELI Suzanne, BA Ibrahima, BERTHEZENE Julien, DANIEL Sandrine, GIANNI Florian, KERSUZAN Alexandre, MONTLIBERT Alexandre, NOBILEAU Delphine and SINNADURAI Saranniya. All the team would like to warmly thank the HYPERVIEW challenge for allowing us to present our results during the IEEE ICIP 2022 conference and to write this collaborative paper.

REFERENCES

[1] R. P. Sishodia, R. L. Ray, and S. K. Singh, "Applications of remote sensing in precision agriculture: A review," *Remote Sensing*, vol. 12, no. 19, 2020.

[2] P. L. Pingali, "Green revolution: Impacts, limits, and the path ahead," *Proceedings of the National Academy of Sciences*, vol. 109, no. 31, pp. 12 302–12 308, 2012.

[3] Y. Song, X. Zhao, H.-Y. Su, B. Li, Y.-M. Hu, and X.-S. Cui, "Predicting spatial variations in soil nutrients with hyperspectral remote sensing at regional scale," *Sensors*, vol. 18, p. 3086, 09 2018.

[4] R. Finger, S. M. Swinton, N. El Benni, and A. Walter, "Precision farming at the nexus of agricultural production and the environment," *Annual Review of Resource Economics*, vol. 11, no. 1, pp. 313–335, 2019.

[5] V. Ponnusamy and S. Natarajan, "Precision agriculture using advanced technology of IoT, unmanned aerial vehicle, augmented reality, and machine learning," in *Smart Sensors for Industrial Internet of Things: Challenges, Solutions and Applications*, D. Gupta, V. Hugo C. de Albuquerque, A. Khanna, and P. L. Mehta, Eds. Cham: Springer International Publishing, 2021, pp. 207–229.

[6] V. M. Sayao, N. V. dos Santos, W. de Sousa Mendes, K. P. Marques, J. L. Safanelli, R. R. Poppiel, and J. A. Demattê, "Land use/land cover changes and bare soil surface temperature monitoring in southeast Brazil," *Geoderma Regional*, vol. 22, p. e00313, 2020. [Online]. Available: https://www.sciencedirect.com/science/article/pii/S2352009420300626

[7] M. Battude, A. Al Bitar, D. Morin, J. Cros, M. Huc, C. Marais Sicre, V. Le Dantec, and V. Demarez, "Estimating maize biomass and yield over large areas using high spatial and temporal resolution Sentinel-2 like remote sensing data," *Remote Sensing of Environment*, vol. 184, pp. 668–681, 2016.

[8] J. Yue, C. Zhou, W. Guo, H. Feng, and K. Xu, "Estimation of winter-wheat above-ground biomass using the wavelet analysis of unmanned aerial vehicle-based digital images and hyperspectral crop canopy images," *International Journal of Remote Sensing*, vol. 42, no. 5, pp. 1602–1622, 2021.

[9] P. Jia, T. Shang, J. Zhang, and Y. Sun, "Inversion of soil pH during the dry and wet seasons in the Yinbei region of Ningxia, China, based on multi-source remote sensing data," *Geoderma Regional*, vol. 25, p. e00399, 2021. [Online]. Available: https://www.sciencedirect.com/science/article/pii/S2352009421000444

[10] E. B. Rutter, D. Ruiz Diaz, and L. M. Hargrave, "Evaluation of Mehlich-3 for determination of cation exchange capacity in Kansas soils," *Soil Science Society of America Journal*, vol. 86, no. 1, pp. 146–156, 2022. [Online]. Available: https://acsess.onlinelibrary.wiley.com/doi/abs/10.1002/saj2.20354

[11] S. Wang, K. Guan, C. Zhang, D. Lee, A. J. Margenot, Y. Ge, J. Peng, W. Zhou, Q. Zhou, and Y. Huang, "Using soil library hyperspectral reflectance and machine learning to predict soil organic carbon: Assessing potential of airborne and spaceborne optical soil sensing," *Remote Sensing of Environment*, vol. 271, p. 112914, 2022.

[12] A. K. Patel, J. K. Ghosh, and S. U. Sayyad, "Fractional abundances study of macronutrients in soil using hyperspectral remote sensing," *Geocarto International*, vol. 37, no. 2, pp. 474–493, 2022.

[13] S. F. Di Gennaro, P. Toscano, M. Gatti, S. Poni, A. Berton, and A. Matese, "Spectral comparison of UAV-based hyper and multispectral cameras for precision viticulture," *Remote Sensing*, vol. 14, no. 3, 2022. [Online]. Available: https://www.mdpi.com/2072-4292/14/3/449

[14] T. W. Ford and S. M. Quiring, "Comparison of contemporary in situ, model, and satellite remote sensing soil moisture with a focus on drought monitoring," *Water Resources Research*, vol. 55, no. 2, pp. 1565–1582, 2019. [Online]. Available: https://agupubs.onlinelibrary.wiley.com/doi/abs/10.1029/2018WR024039

[15] H. Zhang, S. Kariuki, J. L. Schroder, M. E. Payton, and C. Focht, "Interlaboratory Validation of the Mehlich 3 Method for Extraction of Plant-Available Phosphorus," *Journal of AOAC INTERNATIONAL*, vol. 92, no. 1, pp. 91–102, 11 2019. [Online]. Available: https://doi.org/10.1093/jaoac/92.1.91

[16] J. L. Schroder, H. Zhang, J. R. Richards, and M. E. Payton, "Interlaboratory Validation of the Mehlich 3 Method as a Universal Extractant for Plant Nutrients," *Journal of AOAC INTERNATIONAL*, vol. 92, no. 4, pp. 995–1008, 11 2019. [Online]. Available: https://doi.org/10.1093/jaoac/92.4.995

[17] G. Kaur, K. Das, and J. Hazra, "Soil nutrients prediction using remote sensing data in western India: An evaluation of machine learning models," in *IGARSS 2020 - 2020 IEEE International Geoscience and Remote Sensing Symposium*, 2020, pp. 4677–4680.

[18] Z. Wang, Y. Xu, Z. Zhang, and Y. Zhang, "Review: acid mine drainage (AMD) in abandoned coal mines of Shanxi, China," *Water*, vol. 13, no. 1, 2021.

[19] Y. Zhang, C. Xia, X. Zhang, X. Cheng, G. Feng, Y. Wang, and Q. Gao, "Estimating the maize biomass by crop height and narrowband vegetation indices derived from UAV-based hyperspectral images," *Ecol. Indic.*, vol. 129, p. 107985, 2021.

[20] L. Han, G. Yang, H. Dai, B. Xu, H. Yang, H. Feng, Z. Li, and X. Yang, "Modeling maize above-ground biomass based on machine learning approaches using UAV remote-sensing data," *Plant Methods*, vol. 15, no. 10, pp. 1746–4811, 2019.

[21] P. Mazur, D. Gozdowski, W. Stepien, and E. Wojcik-Gront, "Does drone data allow the assessment of phosphorus and potassium in soil based on field experiments with winter rye?" *Agronomy*, vol. 13, no. 2, 2023. [Online]. Available: https://www.mdpi.com/2073-4395/13/2/446

[22] I. Majeed, N. K. Purushothaman, P. Chakraborty, N. Panigrahi, H. B. Vasava, and B. S. Das, "Estimation of soil and crop residue parameters using AVIRIS-NG hyperspectral data," *International Journal of Remote Sensing*, vol. 44, no. 6, pp. 2005–2038, 2023.

[23] M. M. Chitale and S. Kundapura, "High-resolution mapping of soil properties using AVIRIS-NG hyperspectral remote sensing data—a case study over lateritic soils in Mangalore, India," in *Trends in Civil Engineering and Challenges for Sustainability*, M. C. Narasimhan, V. George, G. Udayakumar, and A. Kumar, Eds. Singapore: Springer Singapore, 2021, pp. 735–751.

[24] T. Angelopoulou, S. Chabrillat, S. Pignatti, R. Milewski, K. Karyotis, M. Brell, T. Ruhtz, D. Bochtis, and G. Zalidis, "Evaluation of airborne HySpex and spaceborne PRISMA hyperspectral remote sensing data for soil organic matter and carbonates estimation," *Remote Sensing*, vol. 15, no. 4, 2023. [Online]. Available: https://www.mdpi.com/2072-4292/15/4/1106

[25] X. Meng, Y. Bao, J. Liu, H. Liu, X. Zhang, Y. Zhang, P. Wang, H. Tang, and F. Kong, "Regional soil organic carbon prediction model based on a discrete wavelet analysis of hyperspectral satellite data," *International Journal of Applied Earth Observation and Geoinformation*, vol. 89, p. 102111, 2020.

[26] Y. Hong, S. Chen, Y. Chen, M. Linderman, A. M. Mouazen, Y. Liu, L. Guo, L. Yu, Y. Liu, H. Cheng, and Y. Liu, "Comparing laboratory and airborne hyperspectral data for the estimation and mapping of topsoil organic carbon: Feature selection coupled with random forest," *Soil and Tillage Research*, vol. 199, p. 104589, 2020. [Online]. Available: https://www.sciencedirect.com/science/article/pii/S0167198719307536

[27] S. Ji, C. Zhang, A. Xu, Y. Shi, and Y. Duan, "3D convolutional neural networks for crop classification with multi-temporal remote sensing images," *Remote Sensing*, vol. 10, no. 1, 2018. [Online]. Available: https://www.mdpi.com/2072-4292/10/1/75

[28] D. D. Alexakis, E. Tapoglou, A.-E. K. Vozinaki, and I. K. Tsanis, "Integrated Use of Satellite Remote Sensing, Artificial Neural Networks, Field Spectroscopy, and GIS in Estimating Crucial Soil Parameters in Terms of Soil Erosion," *Remote Sensing*, vol. 11, no. 9, 2019. [Online]. Available: https://www.mdpi.com/2072-4292/11/9/1106

[29] P. Gogumalla, S. Rupavatharam, A. Datta, R. Khopade, P. Choudhari, R. Dhulipala, and S. Dixit, "Detecting soil pH from open-source remote sensing data: A case study of Angul and Balangir Districts, Odisha State," *Journal of the Indian Society of Remote Sensing*, vol. 50, 03 2022.

[30] Z. Liu, Y. Lu, Y. Peng, L. Zhao, G. Wang, and Y. Hu, "Estimation of soil heavy metal content using hyperspectral data," *Remote Sensing*, vol. 11, no. 12, 2019. [Online]. Available: https://www.mdpi.com/2072-4292/11/12/1464

[31] A. Gasmi, C. Gomez, A. Chehbouni, D. Dhiba, and M. El Gharous, "Using PRISMA Hyperspectral Satellite Imagery and GIS Approaches for Soil Fertility Mapping (FertiMap) in Northern Morocco," *Remote Sensing*, vol. 14, no. 16, 2022. [Online]. Available: https://www.mdpi.com/2072-4292/14/16/4080

[32] G. Dhiman, J. Bhattacharya, and S. Roy, "Soil textures and nutrients estimation using remote sensing data in north India - Punjab region," *Procedia Computer Science*, vol. 218, pp. 2041–2048, 2023, international Conference on Machine Learning and Data Engineering. [Online]. Available: https://www.sciencedirect.com/science/article/pii/S1877050923001801

[33] Y. Zhang, B. Sui, H. Shen, and Z. Wang, "Estimating temporal changes in soil pH in the black soil region of Northeast China using remote sensing," *Computers and Electronics in Agriculture*, vol. 154, pp. 204–212, 2018.

[34] A. Bhatta, R. Prasad, D. Chakraborty, J. N. Shaw, J. Lamba, E. Brantley, and H. A. Torbert, "Mehlich 3 as a generic soil test extractant for environmental phosphorus risk assessment across Alabama soil regions," *Agrosystems, Geosciences & Environment*, vol. 4, no. 3, p. e20187, 2021. [Online]. Available: https://acsess.onlinelibrary.wiley.com/doi/abs/10.1002/agg2.20187

[35] M. I. Piha, "Evaluation of Mehlich 3 extractant for estimating phosphorus deficiency and phosphorus sorption of Zimbabwean soils," *Communications in Soil Science and Plant Analysis*, vol. 24, no. 11-12, pp. 1397–1408, 1993. [Online]. Available: https://doi.org/10.1080/00103629309368885

[36] C. Zhang, D. Niu, Y. Ren, and H. Fu, "Extractability of nutrients using Mehlich 3 and ammonium bicarbonate-DTPA methods for selected grassland soils of China," *Plant, Soil and Environment*, vol. 64, no. 9, pp. 448–454, 2018. [Online]. Available: https://pse.agriculturejournals.cz/artkey/pse-201809-0007.php

[37] L. A. Winowiecki, T.-G. Vågen, M. F. Kinnaird, and T. G. O'Brien, "Application of systematic monitoring and mapping techniques: Assessing land restoration potential in semi-arid lands of Kenya," *Geoderma*, vol. 327, pp. 107–118, 2018. [Online]. Available: https://www.sciencedirect.com/science/article/pii/S001670611830510X

[38] A. Jama-Rodzeńska, B. Gałka, A. Szuba-Trznadel, A. Jandy, and J. A. Kamińska, "Effect of struvite (Crystal Green) fertilization on soil element content determined by different methods under soybean cultivation," *Scientific Reports*, vol. 13, no. 1, p. 12702, Aug 2023. [Online]. Available: https://doi.org/10.1038/s41598-023-39753-8

[39] C. Li, S. Wang, M. Sun, D. Li, H. Xu, L. Zhang, C. Xue, W. Ma, and Z. Sun, "Improving the Extraction Process of Mehlich 3 Method for Calcareous Soil Nutrients," *Agronomy*, vol. 12, no. 11, 2022. [Online]. Available: https://www.mdpi.com/2073-4395/12/11/2907

[40] K. Misbah, A. Laamrani, K. Khechba, D. Dhiba, and A. Chehbouni, "Multi-Sensors Remote Sensing Applications for Assessing, Monitoring, and Mapping NPK Content in Soil and Crops in African Agricultural Land," *Remote Sensing*, vol. 14, no. 1, 2022. [Online]. Available: https://www.mdpi.com/2072-4292/14/1/81

[41] L. R. Campos, J. A. Demattê, H. Bellinaso, R. R. Poppiel, L. T. Greschuk, R. Rizzo, N. A. Rosin, and J. T. F. Rosas, "Detection of bare soils in sugarcane areas by temporal satellite images: A monitoring technique for soil security," *Soil Security*, vol. 7, p. 100057, 2022. [Online]. Available: https://www.sciencedirect.com/science/article/pii/S2667006222000247

[42] J. A. M. Demattê, C. T. Fongaro, R. Rizzo, and J. L. Safanelli, "Geospatial Soil Sensing System (GEOS3): A powerful data mining procedure to retrieve soil spectral reflectance from satellite images," *Remote Sensing of Environment*, vol. 212, pp. 161–175, 2018. [Online]. Available: https://www.sciencedirect.com/science/article/pii/S0034425718302049

[43] M. Weiss, F. Jacob, and G. Duveiller, "Remote sensing for agricultural applications: A meta-review," *Remote Sensing of Environment*, vol. 236, p. 111402, 2020.

[44] H. Yu, B. Kong, Q. Wang, X. Liu, and X. Liu, "Hyperspectral remote sensing applications in soil: a review," in *Hyperspectral Remote Sensing*, ser. Earth Observation, P. C. Pandey, P. K. Srivastava, H. Balzter, B. Bhattacharya, and G. P. Petropoulos, Eds. Elsevier, 2020, pp. 269–291.

[45] M. Marcinkiewicz, M. Kawulok, and J. Nalepa, "Segmentation of multispectral data simulated from hyperspectral imagery," in *IGARSS 2019 - 2019 IEEE International Geoscience and Remote Sensing Symposium*, 2019, pp. 3336–3339.

[46] D. Loaiza, C. Aybar, M. Mahecha, F. Martinuzzi, M. Söchting, and S. Wieneke, "A standardized catalogue of spectral indices to advance the use of remote sensing in Earth system research," *Scientific Data*, vol. 10, 04 2023.

[47] N. E. Q. Silvero *et al.*, "Soil variability and quantification based on Sentinel-2 and Landsat-8 bare soil images: A comparison," *Remote Sensing of Environment*, vol. 252, p. 112117, 2021.

[48] X. Jin, Z. Li, H. Feng, Z. Ren, and S. Li, "Deep neural network algorithm for estimating maize biomass based on simulated Sentinel 2A vegetation indices and leaf area index," *Crop Journal*, vol. 8, no. 1, pp. 87–97, 2020.

[49] B. Lu and Y. He, "Evaluating empirical regression, machine learning, and radiative transfer modelling for estimating vegetation chlorophyll content using bi-seasonal hyperspectral images," *Remote Sensing*, vol. 11, no. 17, 2019.

[50] A. Jarocińska, D. Kopeć, M. Kycko, H. Piórkowski, and A. Błońska, "Hyperspectral vs. multispectral data: Comparison of the spectral differentiation capabilities of natura 2000 non-forest habitats," *ISPRS Journal of Photogrammetry and Remote Sensing*, vol. 184, pp. 148–164, 2022. [Online]. Available: https://www.sciencedirect.com/science/article/pii/S0924271622000016

[51] M. Tomaszewski, J. Nalepa, E. Moliszewska, B. Ruszczak, and K. Smykała, "Early detection of solanum lycopersicum diseases from temporally-aggregated hyperspectral measurements using machine learning," *Scientific Reports*, vol. 13, 05 2023.

[52] T. Adão, J. Hruška, L. Pádua, J. Bessa, E. Peres, R. Morais, and J. J. Sousa, "Hyperspectral Imaging: A Review on UAV-Based Sensors, Data Processing and Applications for Agriculture and Forestry," *Remote Sensing*, vol. 9, no. 11, 2017. [Online]. Available: https://www.mdpi.com/2072-4292/9/11/1110

[53] B. Lu, P. D. Dao, J. Liu, Y. He, and J. Shang, "Recent advances of hyperspectral imaging technology and applications in agriculture," *Remote Sensing*, vol. 12, no. 16, 2020.

[54] Z. Cui and J. P. Kerekes, "Potential of red edge spectral bands in future landsat satellites on agroecosystem canopy green leaf area index retrieval," *Remote Sensing*, vol. 10, no. 9, 2018. [Online]. Available: https://www.mdpi.com/2072-4292/10/9/1458

[55] W. Lidberg, M. Nilsson, and A. Ågren, "Using machine learning to generate high-resolution wet area maps for planning forest management: A study in a boreal forest landscape," *AMBIO A Journal of the Human Environment*, vol. 49, 05 2019.

[56] H. Guo, J. Liu, Z. Xiao, and L. Xiao, "Deep CNN-based hyperspectral image classification using discriminative multiple spatial-spectral feature fusion," *Remote Sensing Letters*, vol. 11, no. 9, pp. 827–836, 2020.

[57] G. E. Davies and W. M. Calvin, "Mapping acidic mine waste with seasonal airborne hyperspectral imagery at varying spatial scales," *Environ. Earth Sci.*, vol. 76, 2017.

[58] Y. Yang, Q. Cui, P. Jia, J. Liu, and H. Bai, "Estimating the heavy metal concentrations in topsoil in the Daxigou mining area, China, using multispectral satellite imagery," *Sci. Rep.*, vol. 11, 2021.

[59] N. Wang, L. Xie, Y. Zuo, and S. Wang, "Determination of total phosphorus concentration in water by using visible-near-infrared spectroscopy with machine learning algorithm," *Environmental Science and Pollution Research*, vol. 30, no. 20, pp. 58 243–58 252, 2023. [Online]. Available: https://doi.org/10.1007/s11356-023-26611-3

[60] M. Song, E. Li, C.-I. Chang, Y. Wang, and C. Yu, "Spectral characteristics of nitrogen and phosphorus in water," in *Communications, Signal Processing, and Systems*, Q. Liang, X. Liu, Z. Na, W. Wang, J. Mu, and B. Zhang, Eds. Singapore: Springer Singapore, 2020, pp. 569–578.

[61] N. I. of Standards and Technology, "Strong lines of potassium (k)," 2024, accessed: 2024-03-04. [Online]. Available: https://www.physics.nist.gov/PhysRefData/Handbook/Tables/potassiumtable2.htm

[62] AtomTrace, "Magnesium spectra," 2024, accessed: 2024-03-04. [Online]. Available: https://www.atomtrace.com/elements-database/element/19

[63] L. Hu, M. Zhang, J. Dong, R. Dong, C. Yu, S. Gong, and Z. Yan, "A neoteric dual-channel spectral sensor for wide-range ph detection based on variables in uv–vis peak and intensity," *Anal. Methods*, vol. 13, pp. 5224–5230, 2021. [Online]. Available: http://dx.doi.org/10.1039/D1AY01141C

[64] J. Ma, J. Cheng, J. Wang, R. Pan, F. He, L. Yan, and J. Xiao, "Rapid detection of total nitrogen content in soil based on hyperspectral technology," *Information Processing in*

Agriculture, vol. 9, no. 4, pp. 566–574, 2022. [Online]. Available: https://www.sciencedirect.com/science/article/pii/S2214317321000548

[65] P. Mazur, D. Gozdowski, and E. Wójcik-Gront, "Soil Electrical Conductivity and Satellite-Derived Vegetation Indices for Evaluation of Phosphorus, Potassium and Magnesium Content, pH, and Delineation of Within-Field Management Zones," *Agriculture*, vol. 12, no. 6, 2022. [Online]. Available: https://www.mdpi.com/2077-0472/12/6/883

[66] X. Wang, Y. Zhang, P. M. Atkinson, and H. Yao, "Predicting soil organic carbon content in Spain by combining Landsat TM and ALOS PALSAR images," *International Journal of Applied Earth Observation and Geoinformation*, vol. 92, p. 102182, 2020.

[67] M. Choudhury, J. Christopher, S. Das, A. Apan, N. W. Menzies, S. Chapman, V. Mellor, and Y. P. Dang, "Detection of calcium, magnesium, and chlorophyll variations of wheat genotypes on sodic soils using hyperspectral red edge parameters," *Environmental Technology & Innovation*, vol. 27, p. 102469, 2022.

[68] H. Webb, N. Barnes, S. Powell, and C. Jones, "Does drone remote sensing accurately estimate soil ph in a spring wheat field in southwest montana?" *Precision Agriculture*, vol. 22, 12 2021.

[69] I. Tahmasbian, Z. Xu, S. Boyd, J. Zhou, R. Esmaeilani, R. Che, and S. Hosseini Bai, "Laboratory-based hyperspectral image analysis for predicting soil carbon, nitrogen and their isotopic compositions," *Geoderma*, vol. 330, pp. 254–263, 2018. [Online]. Available: https://www.sciencedirect.com/science/article/pii/S0016706117315732

[70] Y. Peng, L. Wang, L. Zhao, Z. Liu, C. Lin, Y. Hu, and L. Liu, "Estimation of soil nutrient content using hyperspectral data," *Agriculture*, vol. 11, no. 11, 2021. [Online]. Available: https://www.mdpi.com/2077-0472/11/11/1129

[71] A. Singh and K. Gaurav, "Deep learning and data fusion to estimate surface soil moisture from multi-sensor satellite images," *Scientific Reports*, vol. 13, no. 1, p. 2251, Feb 2023. [Online]. Available: https://doi.org/10.1038/s41598-023-28939-9

[72] J. Nalepa, M. Myller, and M. Kawulok, "Training- and test-time data augmentation for hyperspectral image segmentation," *IEEE Geoscience and Remote Sensing Letters*, vol. 17, no. 2, pp. 292–296, 2020.

[73] ——, "Transfer learning for segmenting dimensionally reduced hyperspectral images," *IEEE Geoscience and Remote Sensing Letters*, vol. 17, no. 7, pp. 1228–1232, 2020.

[74] J. Hu, J. Peng, Y. Zhou, D. Xu, R. Zhao, Q. Jiang, T. Fu, F. Wang, and Z. Shi, "Quantitative Estimation of Soil Salinity Using UAV-Borne Hyperspectral and Satellite Multispectral Images," *Remote Sensing*, vol. 11, no. 7, 2019. [Online]. Available: https://www.mdpi.com/2072-4292/11/7/736

[75] J. Nalepa, M. Myller, and M. Kawulok, "Validating hyperspectral image segmentation," *IEEE Geoscience and Remote Sensing Letters*, vol. 16, no. 8, pp. 1264–1268, 2019.

[76] B. Ruszczak, A. M. Wijata, and J. Nalepa, "Unbiasing the estimation of chlorophyll from hyperspectral images: A benchmark dataset, validation procedure and baseline results," *Remote Sensing*, vol. 14, no. 21, 2022. [Online]. Available: https://www.mdpi.com/2072-4292/14/21/5526

[77] S. Kapoor and A. Narayanan, "Leakage and the reproducibility crisis in machine-learning-based science," *Patterns*, Aug. 2023, publisher: Elsevier. [Online]. Available: https://www.cell.com/patterns/abstract/S2666-3899(23)00159-9

[78] G. M. Smith and E. J. Milton, "The use of the empirical line method to calibrate remotely sensed data to reflectance," *International Journal of Remote Sensing*, vol. 20, no. 13, pp. 2653–2662, 1999.

[79] G. P. Anderson *et al.*, "MODTRAN4-based atmospheric correction algorithm: FLAASH (fast line-of-sight atmospheric analysis of spectral hypercubes)," in *ATMHUI VIII*, vol. 4725. SPIE, 2002, pp. 65 – 71.

[80] A. Berk *et al.*, "MODTRAN6: a major upgrade of the MODTRAN radiative transfer code," in *ATMHUI XX*, vol. 9088. SPIE, 2014, pp. 113 – 119.

[81] A. Mehlich, "Mehlich 3 soil test extractant: A modification of Mehlich 2 extractant," *Communications in Soil Science and Plant Analysis*, vol. 15, no. 12, pp. 1409–1416, 1984.

[82] E. A. Hanlon and G. V. Johnson, "Bray/Kurtz, Mehlich III, AB/D and ammonium acetate extractions of P, K and MG in four oklahoma soils," *Communications in Soil Science and Plant Analysis*, vol. 15, no. 3, pp. 277–294, 1984.

[83] T. J. Mattila and G. Ezzati, "A common agricultural soil test can identify legacy P hotspots in a drainage ditch network," *Journal of Environmental Management*, vol. 302, p. 113876, 2022. [Online]. Available: https://www.sciencedirect.com/science/article/pii/S0301479721019381

[84] P. G. Lawrence, W. Roper, T. F. Morris, and K. Guillard, "Guiding soil sampling strategies using classical and spatial statistics: A review," *Agronomy Journal*, vol. 112, no. 1, pp. 493–510, 2020. [Online]. Available: https://acsess.onlinelibrary.wiley.com/doi/abs/10.1002/agj2.20048

[85] J. Nalepa, B. Le Saux, N. Longépé, L. Tulczyjew, M. Myller, M. Kawulok, K. Smykala, and M. Gumiela, "The Hyperview Challenge: Estimating Soil Parameters from Hyperspectral Images," in *2022 IEEE International Conference on Image Processing (ICIP)*, 2022, pp. 4268–4272.

[86] S. Kim and H. Kim, "A new metric of absolute percentage error for intermittent demand forecasts," *International Journal of Forecasting*, vol. 32, no. 3, pp. 669–679, 2016. [Online]. Available: https://www.sciencedirect.com/science/article/pii/S0169207016000121

[87] A. Radford, J. W. Kim, C. Hallacy, A. Ramesh, G. Goh, S. Agarwal, G. Sastry, A. Askell, P. Mishkin, J. Clark *et al.*, "Learning Transferable Visual Models From Natural Language Supervision," in *International Conference on Machine Learning*. PMLR, 2021, pp. 8748–8763.

[88] R. S. Kuzu, F. Albrecht, C. Arnold, R. Kamath, and K. Konen, "Predicting Soil Properties from Hyperspectral Satellite Images," in *2022 IEEE International Conference on Image Processing (ICIP)*. IEEE, 2022, pp. 4296–4300.

[89] A. Dosovitskiy, L. Beyer, A. Kolesnikov, D. Weissenborn, X. Zhai, T. Unterthiner, M. Dehghani, M. Minderer, G. Heigold, S. Gelly *et al.*, "An Image is Worth 16x16 Words: Transformers for Image Recognition at Scale," *arXiv preprint arXiv:2010.11929*, 2020.

[90] K. Han, Y. Wang, H. Chen, X. Chen, J. Guo, Z. Liu, Y. Tang, A. Xiao, C. Xu, Y. Xu, Z. Yang, Y. Zhang, and D. Tao, "A survey on vision transformer," *IEEE Transactions on Pattern Analysis and Machine Intelligence*, vol. 45, no. 01, pp. 87–110, jan 2023.

[91] F. Van Der Meer, "Analysis of spectral absorption features in hyperspectral imagery," *International journal of applied earth observation and geoinformation*, vol. 5, no. 1, pp. 55–68, 2004.

[92] G. R. Mahajan, R. Sahoo, R. Pandey, V. Gupta, and D. Kumar, "Using hyperspectral remote sensing techniques to monitor nitrogen, phosphorus, sulphur and potassium in wheat (triticum aestivum l.)," *Precision agriculture*, vol. 15, pp. 499–522, 2014.

[93] D. Neina, "The role of soil ph in plant nutrition and soil remediation," *Applied and Environmental Soil Science*, vol. 2019, pp. 1–9, 2019.

[94] M.-y. Tian, C.-j. Yu, J.-k. Wang, F. Ding, Z.-h. Chen, N. Jiang, and L.-j. Chen, "Effect of nitrogen additions on soil ph, phosphorus contents and phosphatase activities in grassland," *The Journal of Applied Ecology*, vol. 31, no. 9, pp. 2985–2992, 2020.

[95] H. Meyer, L. W. Lehnert, Y. Wang, C. Reudenbach, T. Nauss, and J. Bendix, "From local spectral measurements to maps of vegetation cover and biomass on the Qinghai-Tibet-Plateau: do we need hyperspectral information?" *International Journal of Applied Earth Observation and Geoinformation*, vol. 55, pp. 21–31, 2017.

[96] N. Meyer, H. Meyer, G. Welp, and W. Amelung, "Soil respiration and its temperature sensitivity (q10): Rapid acquisition using mid-infrared spectroscopy," *Geoderma*, vol. 323, pp. 31–40, 2018.

[97] L. Prokhorenkova, G. Gusev, A. Vorobev, A. V. Dorogush, and A. Gulin, "CatBoost: unbiased boosting with categorical features," in *Advances in Neural Information Processing Systems*, S. Bengio, H. Wallach, H. Larochelle, K. Grauman, N. Cesa-Bianchi, and R. Garnett, Eds., vol. 31. Curran Associates, Inc., 2018, pp. 1–11.

[98] G. Ke, Q. Meng, T. Finley, T. Wang, W. Chen, W. Ma, Q. Ye, and T.-Y. Liu, "LightGBM: A Highly Efficient Gradient Boosting Decision Tree," in *Advances in Neural Information Processing Systems*, I. Guyon, U. V. Luxburg, S. Bengio, H. Wallach, R. Fergus, S. Vishwanathan, and R. Garnett, Eds., vol. 30. Curran Associates, Inc., 2017, pp. 1–9.

[99] F. Pedregosa, G. Varoquaux, A. Gramfort, V. Michel, B. Thirion, O. Grisel, M. Blondel, P. Prettenhofer, R. Weiss, V. Dubourg, J. Vanderplas, A. Passos, D. Cournapeau, M. Brucher, M. Perrot, and E. Duchesnay, "Scikit-learn: Machine learning in Python," *Journal of Machine Learning Research*, vol. 12, pp. 2825–2830, 2011.

[100] R. Caruana, A. Niculescu-Mizil, G. Crew, and A. Ksikes, "Ensemble selection from libraries of models," in *Proceedings of the twenty-first international conference on Machine learning*. ACM, 2004, p. 18.

[101] T. Hastie and R. Tibshirani, "Generalized additive models," *Statistical Science*, vol. 1, no. 3, pp. 297–310, 1986. [Online]. Available: http://www.jstor.org/stable/2245459

[102] X. Meng, Y. Bao, Q. Ye, H. Liu, X. Zhang, H. Tang, and X. Zhang, "Soil organic matter prediction model with satellite hyperspectral image based on optimized denoising method," *Remote Sensing*, vol. 13, no. 12, 2021. [Online]. Available: https://www.mdpi.com/2072-4292/13/12/2273

[103] A. Gholizadeh, L. Boruvka, M. M. Saberioon, J. Kozak, R. Vasat, and K. Nemecek, "Comparing different data preprocessing methods for monitoring soil heavy metals based on soil spectral features," *Soil and Water Research*, vol. 10, no. 4, pp. 218–227, 2015. [Online]. Available: https://swr.agriculturejournals.cz/artkey/swr-201504-0004.php

[104] V. S. F. Garnot, L. Landrieu, S. Giordano, and N. Chehata, "Satellite image time series classification with pixel-set encoders and temporal self-attention," *CoRR*, vol. abs/1911.07757, 2019. [Online]. Available: http://arxiv.org/abs/1911.07757

[105] S. Szymanski, "efficientnet-lite-keras," https://github.com/sebastian-sz/efficientnet-lite-keras, 2021.

[106] M. Tan and Q. V. Le, "Efficientnet: Rethinking model scaling for convolutional neural networks," *CoRR*, vol. abs/1905.11946, 2019. [Online]. Available: http://arxiv.org/abs/1905.11946

[107] Y. Li, H. Zhang, and Q. Shen, "Spectral–spatial classification of hyperspectral imagery with 3d convolutional neural network," *Remote Sensing*, vol. 9, no. 1, 2017. [Online]. Available: https://www.mdpi.com/2072-4292/9/1/67

[108] P. Gavrikov, "visualkeras," https://github.com/paulgavrikov/visualkeras, 2020.

[109] V. Döpper, A. D. Rocha, K. Berger, T. Gränzig, J. Verrelst, B. Kleinschmit, and M. Förster, "Estimating soil moisture content under grassland with hyperspectral data using radiative transfer modelling and machine learning," *International Journal of Applied Earth Observation and Geoinformation*, vol. 110, p. 102817, 2022. [Online]. Available: https://www.sciencedirect.com/science/article/pii/S156984322200019X

[110] X. Jiang, S. Luo, Q. Ye, X. Li, and W. Jiao, "Hyperspectral estimates of soil moisture content incorporating harmonic indicators and machine learning," *Agriculture*, vol. 12, no. 8, 2022. [Online]. Available: https://www.mdpi.com/2077-0472/12/8/1188

[111] A. S. Reis, M. Rodrigues, G. L. Alemparte Abrantes dos Santos, K. Mayara de Oliveira, R. H. Furlanetto, L. G. Teixeira Crusiol, E. Cezar, and M. R. Nanni, "Detection of soil organic matter using hyperspectral imaging sensor combined with multivariate regression modeling procedures," *Remote Sensing Applications: Society and Environment*, vol. 22, p. 100492, 2021. [Online]. Available: https://www.sciencedirect.com/science/article/pii/S2352938521000288

[112] N. J. Anne, A. H. Abd-Elrahman, D. B. Lewis, and N. A. Hewitt, "Modeling soil parameters using hyperspectral image reflectance in subtropical coastal wetlands," *International Journal of Applied Earth Observation and Geoinformation*, vol. 33, pp. 47–56, 2014. [Online]. Available: https://www.sciencedirect.com/science/article/pii/S0303243414000919

[113] D. Datta, M. Paul, M. Murshed, S. W. Teng, and L. Schmidtke, "Comparative analysis of machine and deep learning models for soil properties prediction from hyperspectral visual band," *Environments*, vol. 10, no. 5, 2023. [Online]. Available: https://www.mdpi.com/2076-3298/10/5/77

[114] A. M. Wijata, M.-F. Foulon, Y. Bobichon, R. Vitulli, M. Celesti, R. Camarero, G. Di Cosimo, F. Gascon, N. Longépé, J. Nieke, M. Gumiela, and J. Nalepa, "Taking artificial intelligence into space through objective selection of hyperspectral earth observation applications: To bring the "brain" close to the "eyes" of satellite missions," *IEEE Geoscience and Remote Sensing Magazine*, vol. 11, no. 2, pp. 10–39, 2023.

[115] M. Ziaja, P. Bosowski, M. Myller, G. Gajoch, M. Gumiela, J. Protich, K. Borda, D. Jayaraman, R. Dividino, and J. Nalepa, "Benchmarking deep learning for on-board space applications," *Remote Sensing*, vol. 13, no. 19, 2021. [Online]. Available: https://www.mdpi.com/2072-4292/13/19/3981

[116] J. Nalepa, M. Myller, M. Cwiek, L. Zak, T. Lakota, L. Tulczyjew, and M. Kawulok, "Towards on-board hyperspectral satellite image segmentation: Understanding robustness of deep learning through simulating acquisition conditions," *Remote Sensing*, vol. 13, no. 8, 2021. [Online]. Available: https://www.mdpi.com/2072-4292/13/8/1532

[117] A. Miroszewski, J. Mielczarek, G. Czelusta, F. Szczepanek, B. Grabowski, B. Le Saux, and J. Nalepa, "Detecting Clouds in Multispectral Satellite Images Using Quantum-Kernel Support Vector Machines," *IEEE Journal of Selected Topics in Applied Earth Observations and Remote Sensing*, vol. 16, pp. 7601–7613, 2023.

[118] S. Avagyan, V. Katkovnik, and K. Egiazarian, "RAW2HSI: Learning-Based Hyperspectral Image Reconstruction from Low-Resolution Noisy Raw-RGB," in *2023 International Symposium on Image and Signal Processing and Analysis (ISPA)*, 2023, pp. 1–6.

[119] J. Kowalewski, J. Domaradzki, M. Zieba, and M. Podgórski, "Hyperspectral imaging – a short review of methods and applications," *Metrology and Measurement Systems*, vol. vol. 30, no. No 4, pp. 637–354, 2023. [Online]. Available: http://journals.pan.pl/Content/130305/art03_int.pdf

[120] A. Miroszewski, J. Mielczarek, F. Szczepanek, G. Czelusta, B. Grabowski, B. L. Saux, and J. Nalepa, "Cloud Detection in Multispectral Satellite Images Using Support Vector Machines with Quantum Kernels," in *IGARSS 2023 - 2023 IEEE International Geoscience and Remote Sensing Symposium*, 2023, pp. 796–799.

[121] A. Patel, L. Khedikar, M. Lokakshi, and S. Khandelwal, "FarmO'Cart: Multilingual Voice-Assisted Machine Learning Based real-time price Prediction to Enhance Agricultural Income," in *2023 4th International Conference on Electronics and Sustainable Communication Systems (ICESC)*, 2023, pp. 1328–1333.

[122] M. Wan, T. Yan, G. Xu, A. Liu, Y. Zhou, H. Wang, and X. Jin, "MAE-NIR: A masked autoencoder that enhances near-infrared spectral data to predict soil properties," *Computers and Electronics in Agriculture*, vol. 215, p. 108427, 2023. [Online]. Available: https://www.sciencedirect.com/science/article/pii/S0168169923008153

[123] B. Grabowski, M. Ziaja, M. Kawulok, P. Bosowski, N. Longépé, B. Le Saux, and J. Nalepa, "Squeezing adaptive deep learning methods with knowledge distillation for on-board cloud detection," *Engineering Applications of Artificial Intelligence*, vol. 132, p. 107835, 2024. [Online]. Available: https://www.sciencedirect.com/science/article/pii/S0952197623020195

[124] H. Li, W. Ju, Y. Song, Y. Cao, W. Yang, and M. Li, "Soil organic matter content prediction based on two-branch convolutional neural network combining image and spectral features," *Computers and Electronics in Agriculture*, vol. 217, p. 108561, 2024. [Online]. Available: https://www.sciencedirect.com/science/article/pii/S0168169923009493

[125] G. Bolar, D. Joshi, S. P. Chennamsetti, and S. Gurugopinath, "Performance Comparison of Learning Methods for Soil Parameter Estimation using Hyperspectral Data," in *2022 8th International Conference on Signal Processing and Communication (ICSC)*, 2022, pp. 479–484.

[126] J. Charyton, "Soil elements regression based on Hyperspectral data using Attention-Aided CNNs," Ph.D. dissertation, 08 2022. [Online]. Available: http://dx.doi.org/10.13140/RG.2.2.33158.45124

[127] X. Zhang and L. Han, "A Generic Self-Supervised Learning (SSL) Framework for Representation Learning from Spectral–Spatial Features of Unlabeled Remote Sensing Imagery," *Remote Sensing*, vol. 15, no. 21, 2023. [Online]. Available: https://www.mdpi.com/2072-4292/15/21/5238

[128] X. Zhao, Z. Xiong, and X. Zhu, "Soil Parameters Prediction from Hyperspectral Images via Multitask Learning," in *EGU General Assembly 2023, Vienna, Austria, 24–28 April 2023*, 2023, pp. EGU23–2439. [Online]. Available: https://doi.org/10.5194/egusphere-egu23-2439

[129] V. Zaigrajew, H. Baniecki, L. Tulczyjew, A. M. Wijata, J. Nalepa, N. Longépé, and P. Biecek, "Red Teaming Models for Hyperspectral Image Analysis Using Explainable AI," *CoRR*, vol. abs/2403.08017, 2024. [Online]. Available: https://arxiv.org/abs/2403.08017

Jakub Nalepa received his M.Sc. (2011), Ph.D. (2016), and D.Sc. (2021) degrees in computer science from Silesian University of Technology, 44-100 Gliwice, Poland, where he is currently an associate professor. He is also the head of artificial intelligence (AI) at KP Labs, 44-100 Gliwice, Poland, where he shapes the scientific and industrial AI objectives of the company. He has been pivotal in designing the onboard deep learning capabilities of Intuition-1 and has contributed to other missions, including CHIME, Φ-Sat-2 and OPS-SAT. His research interests include (deep) machine learning, hyperspectral data analysis, signal processing, remote sensing, and tackling practical challenges that arise in Earth observation to deploy scalable solutions. He was the general chair of the HYPERVIEW Challenge at the 2022 IEEE International Conference on Image Processing, focusing on the estimation of soil parameters from hyperspectral images onboard Intuition-1 to maintain farm sustainability by improving agricultural practices. He is a Senior Member of IEEE.